Naval Research Laboratory
Washington, DC 20375-5000

NRL Memorandum Report 6352

Environmental Measurements in the McKinley Climatic Laboratory Main Chamber, May 2-10, 1988

G. M. FRICK AND W. A. HOPPEL

Atmospheric Physics Branch
Space Sciences Division

October 5, 1988

SECURITY CLASSIFICATION OF THIS PAGE

REPORT DOCUMENTATION PAGE

Form Approved
OMB No 0704-0188

1a REPORT SECURITY CLASSIFICATION UNCLASSIFIED	1b RESTRICTIVE MARKINGS
2a SECURITY CLASSIFICATION AUTHORITY	3 DISTRIBUTION / AVAILABILITY OF REPORT Approved for public release; distribution unlimited.
2b DECLASSIFICATION / DOWNGRADING SCHEDULE	
4 PERFORMING ORGANIZATION REPORT NUMBER(S) NRL Memorandum Report 6352	5 MONITORING ORGANIZATION REPORT NUMBER(S)
6a NAME OF PERFORMING ORGANIZATION Naval Research Laboratory 6b OFFICE SYMBOL (If applicable) Code 4110	7a NAME OF MONITORING ORGANIZATION
6c ADDRESS (City, State, and ZIP Code) Washington, DC 20375-5000	7b ADDRESS (City, State, and ZIP Code)
8a NAME OF FUNDING / SPONSORING ORGANIZATION Office of Naval Research 8b OFFICE SYMBOL (If applicable)	9 PROCUREMENT INSTRUMENT IDENTIFICATION NUMBER
8c ADDRESS (City, State, and ZIP Code) Arlington, VA 22217	10 SOURCE OF FUNDING NUMBERS PROGRAM ELEMENT NO 61153N; PROJECT NO RR033-02-42; TASK NO; WORK UNIT ACCESSION NO DN480-215

11 TITLE (Include Security Classification)
Environmental Measurements in the McKinley Climatic Laboratory Main Chamber, May 2-10, 1988

12 PERSONAL AUTHOR(S)
Frick, G.M. and Hoppel, W.A.

13a TYPE OF REPORT	13b TIME COVERED	14 DATE OF REPORT (Year, Month, Day)	15 PAGE COUNT
Interim	FROM _____ TO _____	1988 October 5	76

16 SUPPLEMENTARY NOTATION

17 COSATI CODES		
FIELD	GROUP	SUB-GROUP

18 SUBJECT TERMS (Continue on reverse if necessary and identify by block number)
Helium Neon

19 ABSTRACT (Continue on reverse if necessary and identify by block number)

Environmental measurements were made in the main chamber of the McKinley Climatic Laboratory at Eglin AFB, Florida, to help assess the performance of HARM DSU-19 target detectors. The measurements revealed that the depolarization of backscatter from a He-Ne laser was significantly greater for an ice fog than a wet fog.

20 DISTRIBUTION / AVAILABILITY OF ABSTRACT	21 ABSTRACT SECURITY CLASSIFICATION
☒ UNCLASSIFIED/UNLIMITED ☐ SAME AS RPT ☐ DTIC USERS	UNCLASSIFIED

22a NAME OF RESPONSIBLE INDIVIDUAL	22b TELEPHONE (Include Area Code)	22c OFFICE SYMBOL
G.M. Frick	(202) 767-3589	Code 4110

DD Form 1473, JUN 86 Previous editions are obsolete SECURITY CLASSIFICATION OF THIS PAGE

S/N 0102-LF-014-6603

CONTENTS

ENVIRONMENTAL MEASUREMENTS IN THE MCKINLEY CLIMATIC LABORATORY MAIN CHAMBER, MAY 2-10, 1988

I. INTRODUCTION

A. Purpose

These measurements were made in support of the evaluation of HARM DSU-19 target detectors (TDs). The TDs illuminate a volume using an infrared laser diode and look at the backscattered signal. It is possible that certain atmospheric conditions may cause backscatter such that fuzing will occur. Measurement of the environment in terms of visibility, aerosol particle distribution and water or ice content define parameters which could hinder the performance of the TDs.

B. Facility and Instrumentation

The measurements were made in the main chamber of the McKinley Climatic Laboratory, located on Eglin AFB, Florida. The chamber has a volume of approximately 3,000,000 cubic feet, and can be cooled to -65 degrees Farenheit. Rain was simulated by arrays of nozzles situated approximately 40 feet above the chamber floor, which produced rain rates up to five inches per hour over an area approximately 50 x 100 ft. Both wet and ice fogs were created by bringing in warm humid air through an air handler at the top of the chamber and mixing it with the cooled chamber air using a large wind machine, two snow machine fans helped to distribute the fog throughout the chamber.

Rain rates were measured with a tipping bucket rain gauge, along with occasional comparisons to a standard rain gauge. Rain droplets were sized by impaction on a powdered mesh which was photographed for later evaluation. The mist component of the rain ($10 \leq r \leq 150 \mu m$) was measured with a Particle Measuring Systems (PMS) Optical Array Probe (OAP). The OAP was also used in fogs, along with a PMS Classical Scattering Aerosol Spectrometer Probe (CSASP) which covered the range $1 \leq r \leq 10 \mu m$, to obtain size distributions and estimates of the liquid water or ice content of the fogs..

Visibility measurements were made with a HSS VR-301 visiometer, this instrument provided values for the visual range (VR) which were in close agreement with a range of visual targets.

An instrument was built by NRL, specifically for these tests, to measure the intensities of the parallel and cross polarization components of backscattered light from a He-Ne laser. This instrument was operated during the ice and wet fogs and provided an indication of the depolarization produced by the fogs when the visual range was less than approximately 30 meters.

C. Theory of Fog Formation by Air Mass Mixing

In order to estimate the amount of warm humid air required to produce fogs of a certain temperature and density for a given chamber temperature, a few calculations were necessary; the first being the saturation vapor pressure for water.

Manuscript approved August 1, 1988.

The saturation vapor pressures over water and ice are given by the Goff-Gratch formulas:

$$\log_{10} e_w = -7.90298 \left[\frac{T_s}{T} - 1\right] + 5.02808 \log_{10} \left[\frac{T_s}{T}\right]$$

$$- 1.3816 \times 10^{-7} \left[10^{11.344(1-T/T_s)} - 1\right]$$

$$+ 8.1328 \times 10^{-3} \left[10^{-3.49149(T_s/T - 1)} - 1\right] + \log_{10} e_{ws}$$

for water, and

$$\log_{10} e_i = - 9.09718 (T_o/T - 1) - 3.56654 \log_{10} (T_o/T)$$

$$+ 0.876793 (1 - T/T_o) + \log_{10} e_{io}$$

for ice.

where e_w = SVP (mb) over water

e_i = SVP (mb) over ice

T = Absolute Temperature (°K)

T_o = 273.16 °K

T_s = 373.16 °K

e_{ws} = SVP @ T_s (1013.25 mb for std. atm.)

e_{io} = SVP @ T_o (6.1071 mb = 0.0060273 std. atm.)

These formulas are plotted in Fig. 1.

The mixing of two saturated air masses results in a maximum vapor pressure given by:

$$e_{mix} = \frac{M_1 e_1 + M_2 e_2}{M_1 + M_2} \quad \text{at} \quad T_{mix} = \frac{M_1 T_1 + M_2 T_2}{M_1 + M_2}$$

where e_{mix} = vapor pressure of the mixture

e_1 = saturation vapor pressure at T_1

e_2 = saturation vapor pressure at T_2

T_1 = Temperature of the warm air

T_2 = Temperature of the cold air

M_1 = Mass of the humid air at temperature T_1 (= $M_{1a} + M_{1v}$)

M_2 = Mass of the dry air at temperature T_2 (= M_{2a})

Thus if droplet formation is inhibited, the vapor pressure of the mixture will lie along a straight line connecting the saturation vapor pressures e_1 and e_2 obtained from Fig. 1.

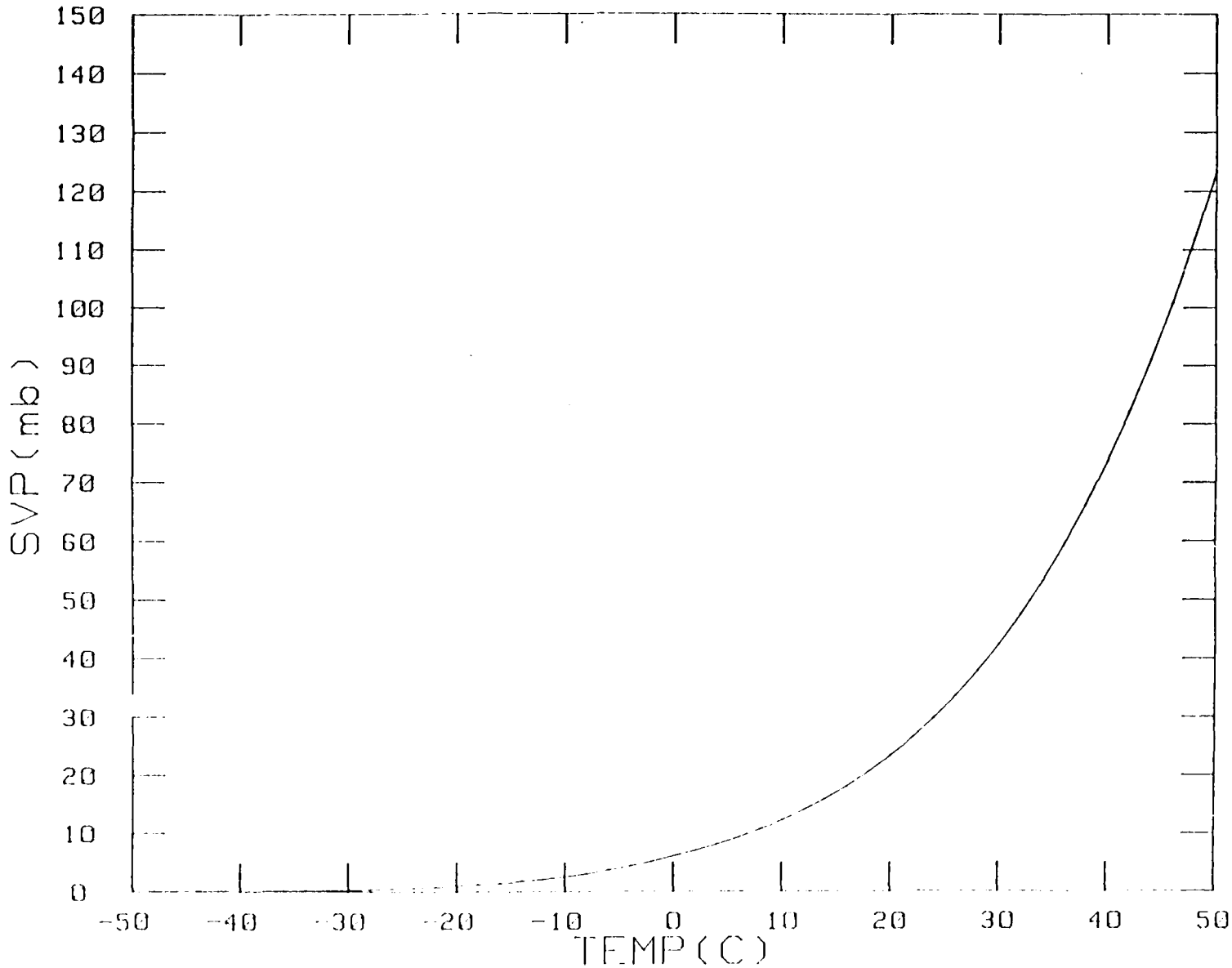

Fig. 1 Saturation vapor pressure vs. temperature.

Since the saturation vapor pressure curve is slightly concave, this will always produce a supersaturation. As fog droplets are formed, the latent heat warms the mixture and decreases the supersaturation which inhibits further growth. The final temperature and liquid water content (LWC) can be computed by solving heat balance equations for the two air masses, including the latent heat of the water vapor.
Let

M_{1vi} = Initial mass of water vapor

M_{1vf} = Final mass of water vapor

C_{pa} = Specific heat of dry air

C_{pv} = Specific heat of water vapor

C_{pw} = Specific heat of water

L = Latent heat of vaporization of water

$$Q_1 = C_{pa} M_{1a}(T_1 - T_f) + C_{pv} M_{1vf}(T_1 - T_f) - L (M_{1vi} - M_{1vf}) + C_{pw} (M_{1vi} - M_{1vf}) (T_1 - T_f)$$

Neglecting the second and fourth terms because they are relatively small

$$Q_1 = C_{pa} M_{1a} (T_1 - T_f) - L (M_{1vi} - M_{1vf})$$

and for the cold, dry air mass

$$Q_2 = M_2 C_{pa} (T_f - T_2)$$

now $Q_1 - Q_2 = 0$, so

Balance the heat lost by the warmer air to that gained by the cooler air.

$$C_{pa} M_{1a} (T_1 - T_f) + L (M_{1vi} - M_{1vf}) - M_2 C_{pa} (T_f - T_2) = 0 \qquad (1)$$

The water mixing ratio, w, is the mass of the water vapor divided by the mass of the dry air. Thus

$$w = \frac{M_v}{M_a} = \frac{0.622\ e}{p - e} \simeq \frac{0.622\ e}{p}$$ where

e = Partial pressure of water vapor

p = Total pressure (= 1013 mb)

now $M_{1vi} = M_{1a}\, w(T_1)$ and $M_{1vf} = M_{1a}\, w(T_f)$ so that eq. (1) becomes

$$M_{1a} \{ C_{pa} (T_1 - T_f) - L [w(T_1) - w(T_f)] \} + M_2 C_{pa} (T_f - T_2) = 0$$

now the change in mixing ratio, $\Delta w = w(T_1) - w(T_f)$

$$= \frac{0.622}{1013} [e_w(T_1) - e_w(T_f)]$$

where $e_w(T)$ can be obtained from the Goff-Gratch formula.

Let $f_1 = \frac{M_{1a}}{M_{1a} + M_2}$ and $f_2 = \frac{M_2}{M_{1a} + M_2}$, then

$$f_1 \{C_{pa}(T_f - T_1) + L \frac{0.622}{1013} [e_w(T_f) - e_w(T_1)]\} + f_2 C_{pa}(T_f - T_2) = 0$$

Once f_1, f_2, T_1 and T_2 are set, since C_{pa}, L and $e_w(T_1)$ are known, T_f can be determined by a simple iterative process.

The LWC can be approximately determined by the relation

$$LWC\ (g/m^3) = \frac{3.53 \times 10^5\, w}{T (1 + 0.61\, w)}$$

Fig. 2 shows the predicted LWC and final temperatures for mixtures of 10% warm saturated air at temperature T_1 (given on the abscissa), with cold dry air at the temperatures labeled on the curves. The solid lines give the final temperature, read on the left hand side of the figure, and the solid lines give the LWC, read on the right. For example; 10% warm saturated air at 30°C mixed with 90% dry air at 0°C would result in a final temperature of 7.9°C and a LWC of 2.4 g/m^3.

D. Visibility Relations to the Fog and Rain Microstructure

Almost all of particulate scattering theory has been limited to spherical particles. The visual range through a population of spherical particles can be expressed in terms of the scattering coefficient σ, and the liminal contrast ϵ as:

$$\text{visual range} = \frac{\ln |1/\epsilon|}{\sigma}$$

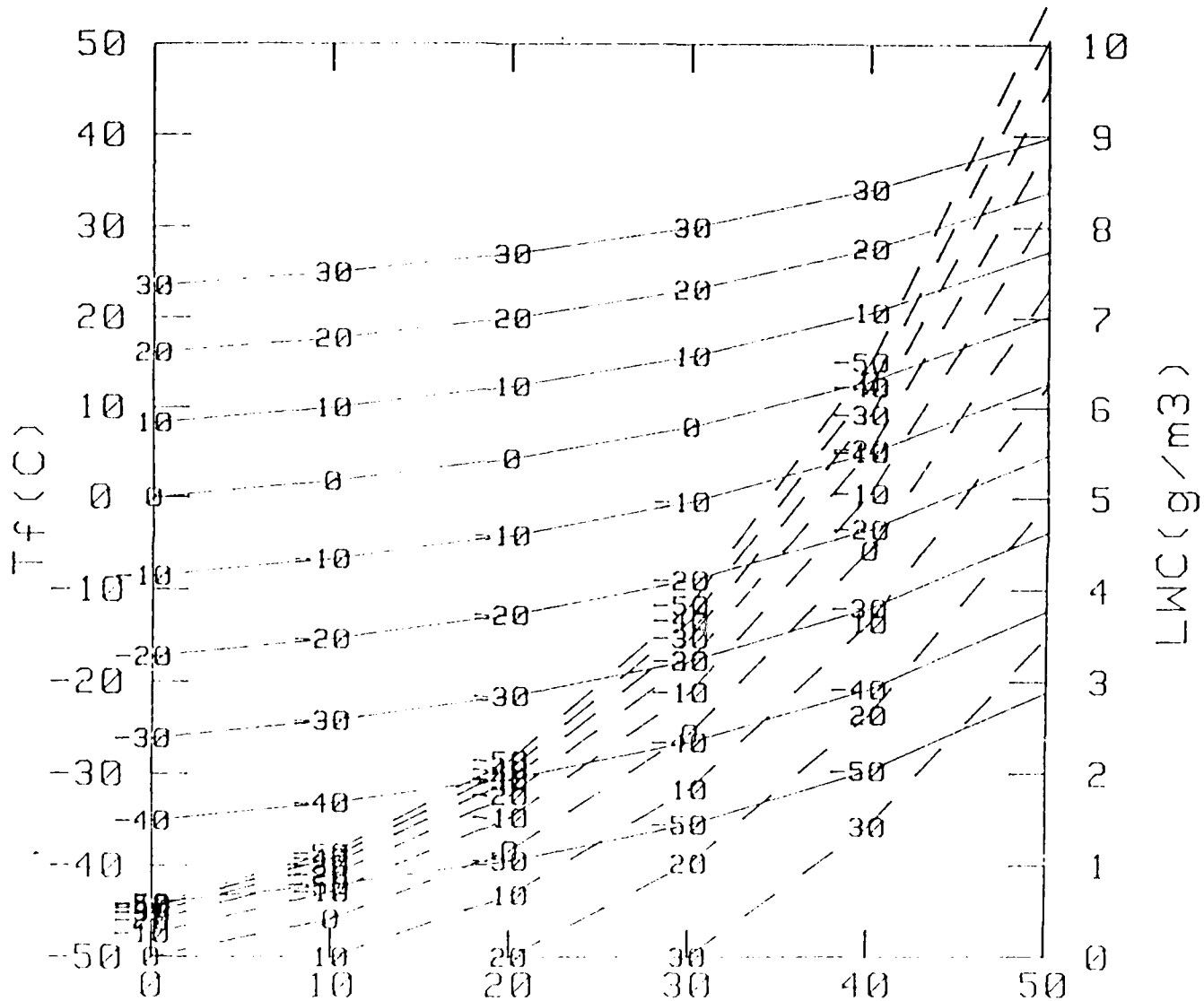

Fig. 2 Predicted LWC for 10% saturated air at T1 mixed with cold dry air at various temperatures.

We have set $\ln |1/\epsilon| = 3.00$ to be consistant with the formula used

with the HSS visiometer, and calculated σ from

$$\sigma = \sum_{i=1}^{N} \sigma_i = 2\pi \sum_{i=1}^{N} n_i r_i^2$$

where n_i is the concentration (m^{-3}) of particles with radius r_i (m),

as obtained from the PMS instruments. The calculated visual range can then be compared to that obtained from the HSS visiometer. A plot of visibility and LWC vs. concentration of monodisperse water droplets is presented in Fig. 3. The visibility is given by the solid lines (decreasing with particle concentration) and the LWC is given by the dotted lines (increasing with particle concentration).

E. Polarization Measurements

An instrument to measure the polarization of backscattered light from ice and wet fogs was specially constructed for these tests. The instrument consists of a He-Ne laser which illuminates the fog with a polarized beam, and a receiver that looks at the backscattered laser light, splits it into components with polarization parallel and perpendicular to the outgoing beam, and provides voltage outputs proportional to their intensities. This allows calculation of the polarization of the backscattered light in terms of the output voltages. Thus

$$\% \text{ Polarization} = \frac{Vo - Vx}{Vo + Vx}$$

where Vo (Vx) is the voltage output proportional to the intensity of backscattered light parallel (perpendicular) to the outgoing beam.

II. TESTS

A. Rain

The rain tests were conducted May 2-4 using two sets of spray nozzles. The tests of May 2 and 3 used the smaller nozzles which provided rain rates from 0.8 to 1.9 in/hr The May 4 test used larger nozzles, giving rates from 1.4 to 5.0 in/hr. The spray from the nozzles produced a considerable amount of fine mist, especially for the larger rain rates. The PMS OAP was used on May 3-4 to size the droplet whose radii were between 10 and 150 microns. The powdered mesh method was used to size the larger droplets, however when the rain rate was greater than about 2.5 in/hr the droplets were too small and too numerous for this method to work satisfactorily. Figures 4, 5 and 6 are histograms of droplet size distributions for the rain rates of 0.8, 1.4 and 2.5 in/hr respectively. Figure 4 is for the smaller nozzles, figures 5 and 6 are for the larger nozzles. The portions for $r < 150$ μm are derived directly from the OAP data, while the larger portion is calculated from the rain rate,

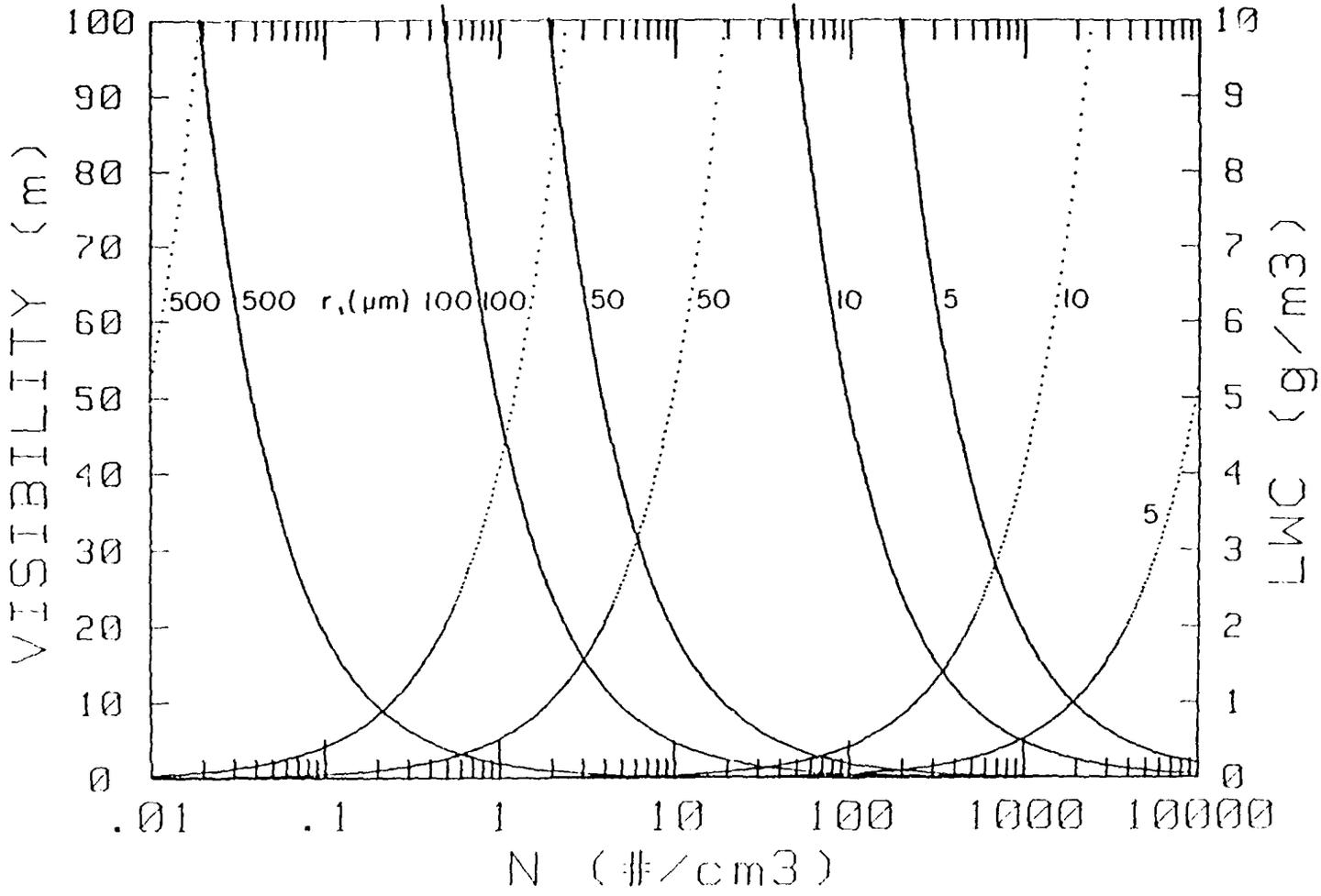

Fig. 3 Visibility and LWC vs. monodisperse droplet concentration.

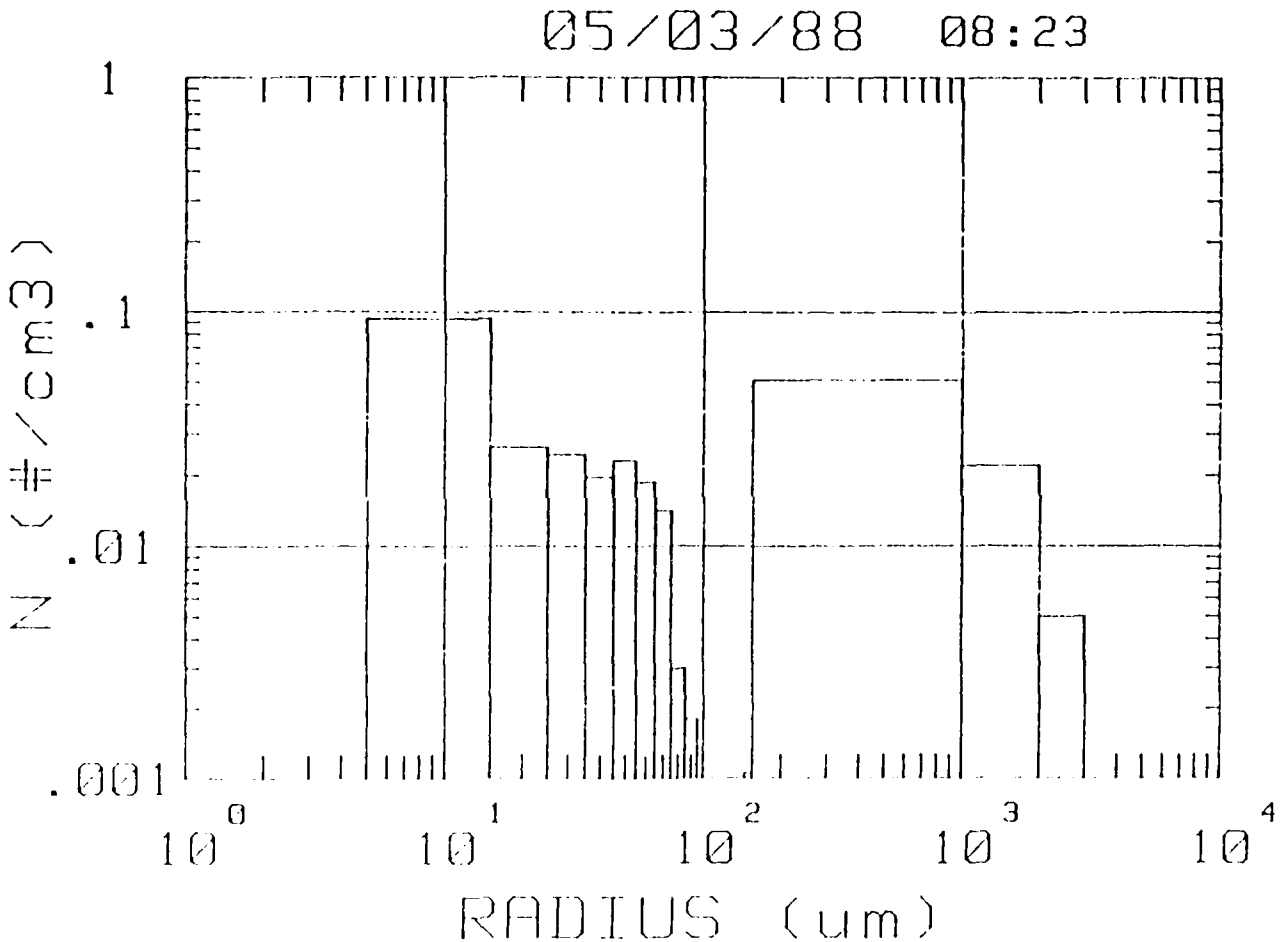

Fig. 4 Histogram of droplet sizes for rain rate of 0.8 in/hr.

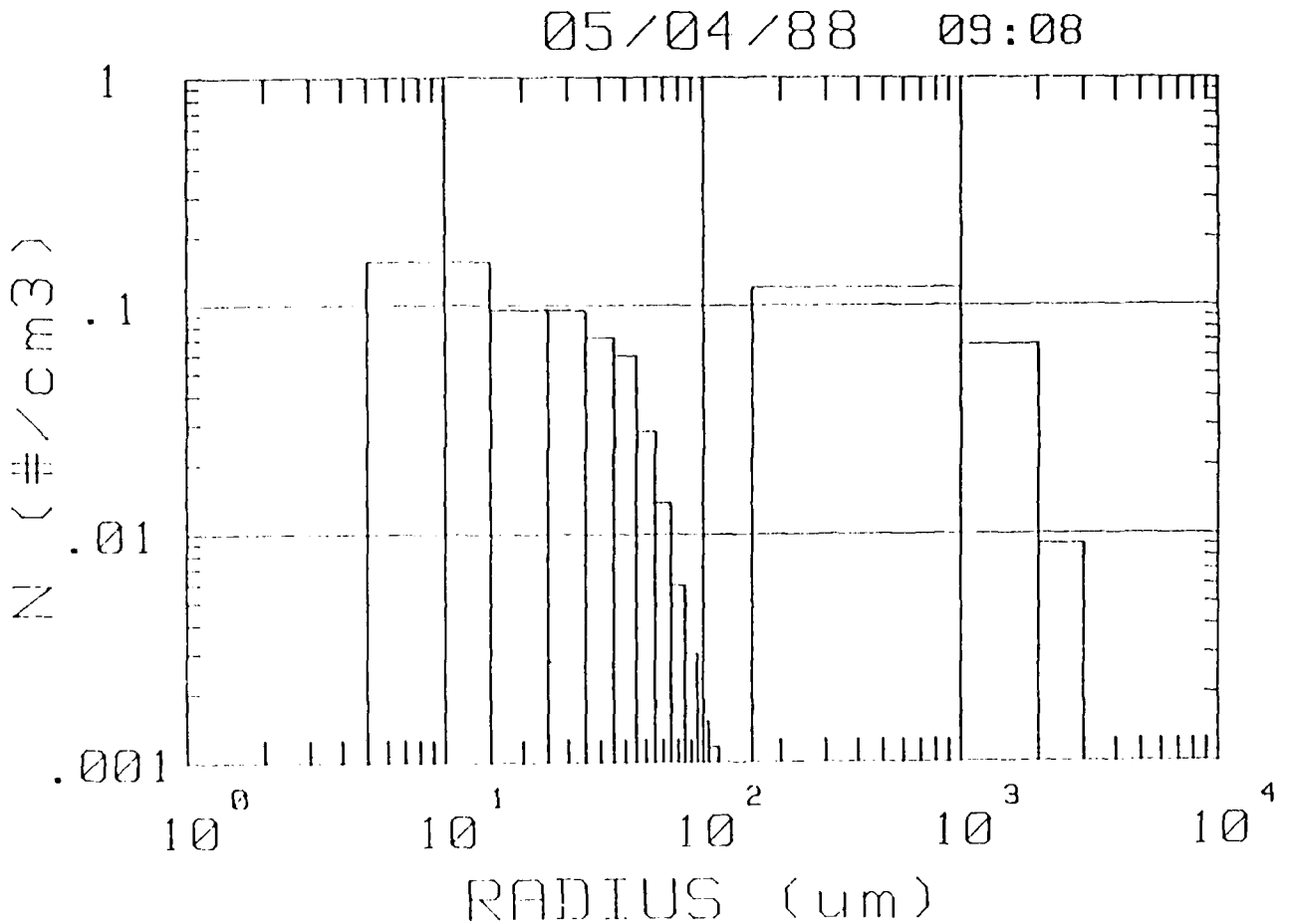

Fig. 5 Histogram of droplet sizes for rain rate of 1.4 in/hr.

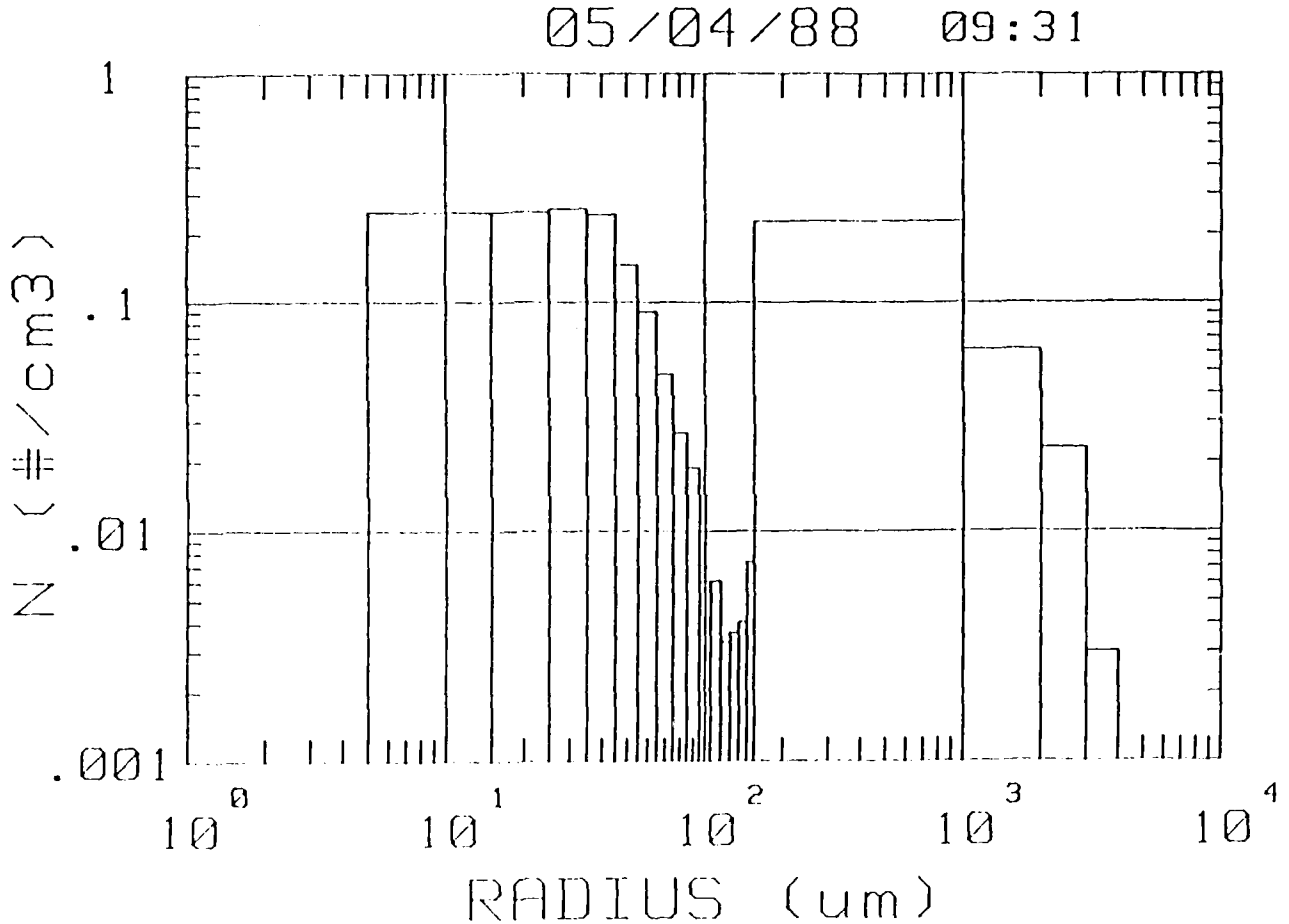

Fig. 6 Histogram of droplet sizes for rain rate of 2.5 in/hr.

fall velocities and droplet size distribution from the powdered mesh. Table 1 gives a synopsis of the rain data, and plots of the visual range during the rain tests are presented in Appendix A. The lack of a direct correlation between rain rate and visibility is evident from Table 1, this is because the droplet size distribution is dependent upon the flow through the nozzles. Figure 7 shows two size distributions obtained from the OAP data for the rain rates of 1.1 in/hr (curve A) and 1.0 in/hr (curve B). Curve B has many more small droplets (these are responsible for the reduction in visibility) because the flow rate through the nozzles was greater, producing a higher degree of atomization. The rain rate for curve B is less than for curve A because the smaller droplets drift a considerable distance and distribute the water over a much larger area.

Table 1.

TIME	RAIN RATE (in/hr)	VISUAL RANGE (m)	
	5/2/88 small nozzles		
1246-1251	0.6	300	
1252-1254	1.0	150	
1301-1308	1.0	70	
1311-1318	1.2	40	
1322-1329	1.5	22	
1332-1341	1.5	19	
1349-1406	1.9	15	
	5/3/88		
0821-0827	0.8	210	
0833-0843	1.1	150	
0851-0902	1.0	50	
0904-0919	1.3	35	
0921-0935	1.7	18	
	5/4/88 large nozzles		
0908-0916	1.4	125	
0920-0935	2.5	55	
0941-0948	2.9	40	
0952-1007	4.4	30	
1012-1034	4.8	16	
1043-1050	1.4	100	
1051-1100	2.1	60	(est.)
1102-1107	2.8	35	
1115-1125	3.5	25	
1133-1143	5.0	12	

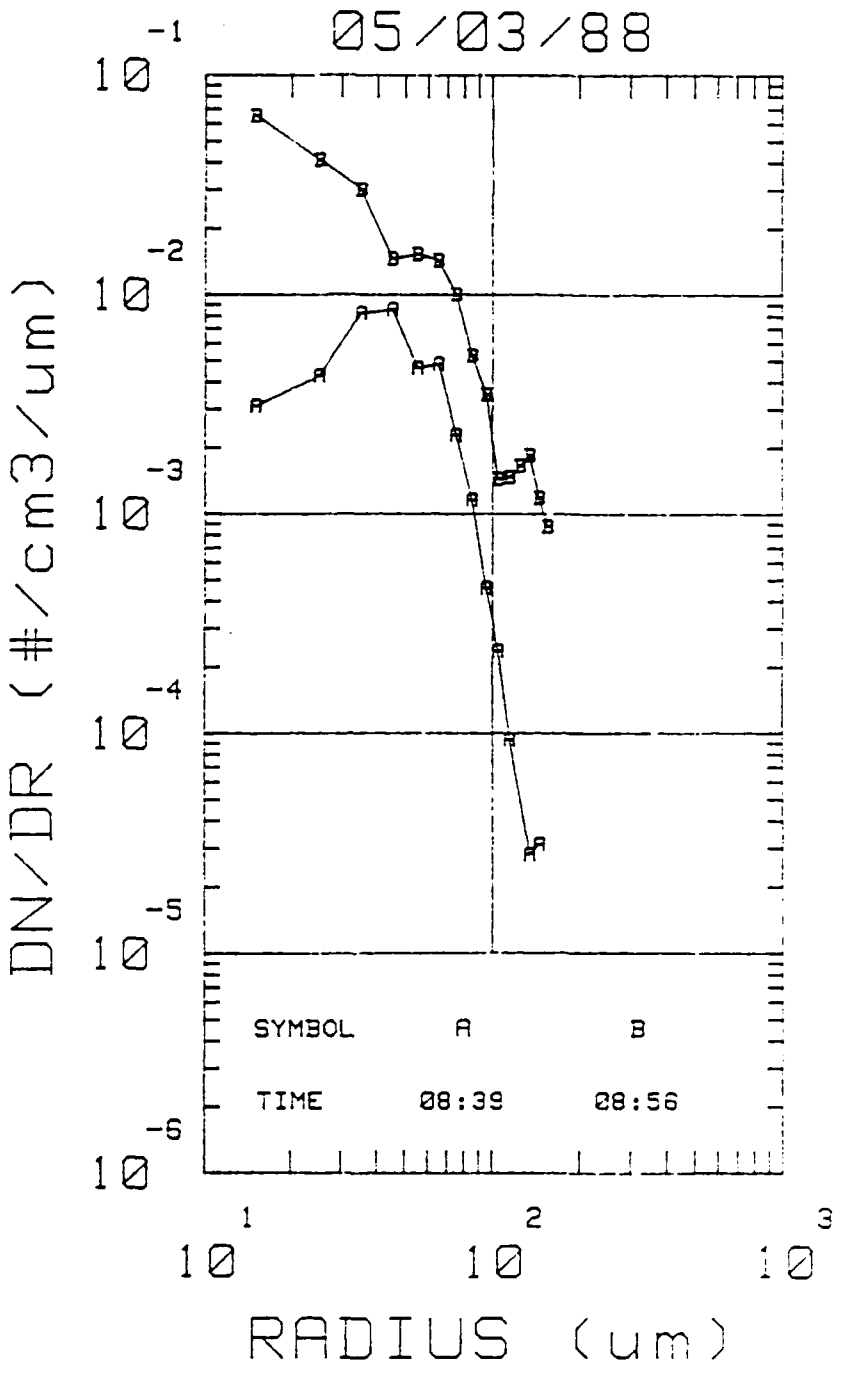

Fig. 7 Size distributions for rain rates of 1.1 (A) and 1.0 (B) in/hr.

B. Ice Fog

The ice fog tests were conducted on May 6, upon our arrival at the chamber that morning we observed the chamber was already foggy. This was purported to be due to an opening of the large chamber door earlier that morning. Upon entering our shelter in the chamber at about 1245 we recorded the visual range to be approximately 80 m and the temperature as -48 °C. The very low temperature ensured that the particles were ice, as was visually confirmed by their glint in the laser beam. At about 1344, as the warm humid air was brought in, the region in front of the wind machine had the appearance of a heavy snowstorm. Snow built up on and fell from the ceiling trusses of the vicinity of the wind machine. Within five minutes the chamber was filled with a heavy ice fog and frost formed on all available surfaces. At 1354 this first ice fog yielded a minimum visibility of 23 meters before it began to dissipate, during this time the chamber temperature rose to -43.2°C. A second fog, created by injecting more warm humid air at 1429, produced a minimum visibility of 41 m and brought the chamber temperature up to -33.3°C. Silver iodide was burned and more humid air was injected at 1448, this time we obtained a minimum visibility of only 45 m. Plots of the recorded visibilities are given in Figs. 8 and 9.

The most interesting data from this test is that from the polarization instrument, unfortunately this instrument only obtains adequate backscatter when the visibility is less than about 30 m. Thus the first ice fog was the only one to yield polarization data. Fig. 10 shows the polarization and voltage outputs from the instrument for the times shown. The polarization is given by the histograms and the O's (X's) denote the output voltages from the parallel (perpendicular) component. Figure 10 is of particular interest, for it shows that the ice fog did not simply depolarize the laser beam, but repolarized it in a direction perpendicular to original polarization. We believe this to be due to the scattering of the beam by non-spherical (probably needle-like) ice crystals which could have a large amount of internal reflection and a preferred orientation during their fall. The ice content of these fogs, given in Figures 11-13, was computed from the CAP and CSAS data and assumes solid spherical particles. The maximum ice content of 1.9 cm^3/m^3 achieved during the first ice fog corresponds to a visibility of 23 m. Figure 14 give the size distributions of ice crystals for the times 1354, 1400 and 1404. These show the peak particle size to be at r=4 μm, but give no indication of any distinguishing characteristic that set curves A and C apart from curve B, as revealed by the differences in the polarization data (specifically the Xs) of Fig. 10. Figure 15 shows the size distributions at the times of maximum ice content for the three ice fogs. Curve A corresponds to a visibility of 24 m and an ice content (IC) of 1.9 cm^3/m^3, curve B is for VR=41 m, IC=3.3 cm^3/m^3 and curve C is for VR=45 m, IC=3.0 cm^3/m^3.

C. Wet Fogs

The wet fogs were produced in a manner identical to the ice fogs, except the initial chamber temperature was held close to freezing. On May 9 the initial chamber was -10°C and we injected saturated air at 18°C at a rate of

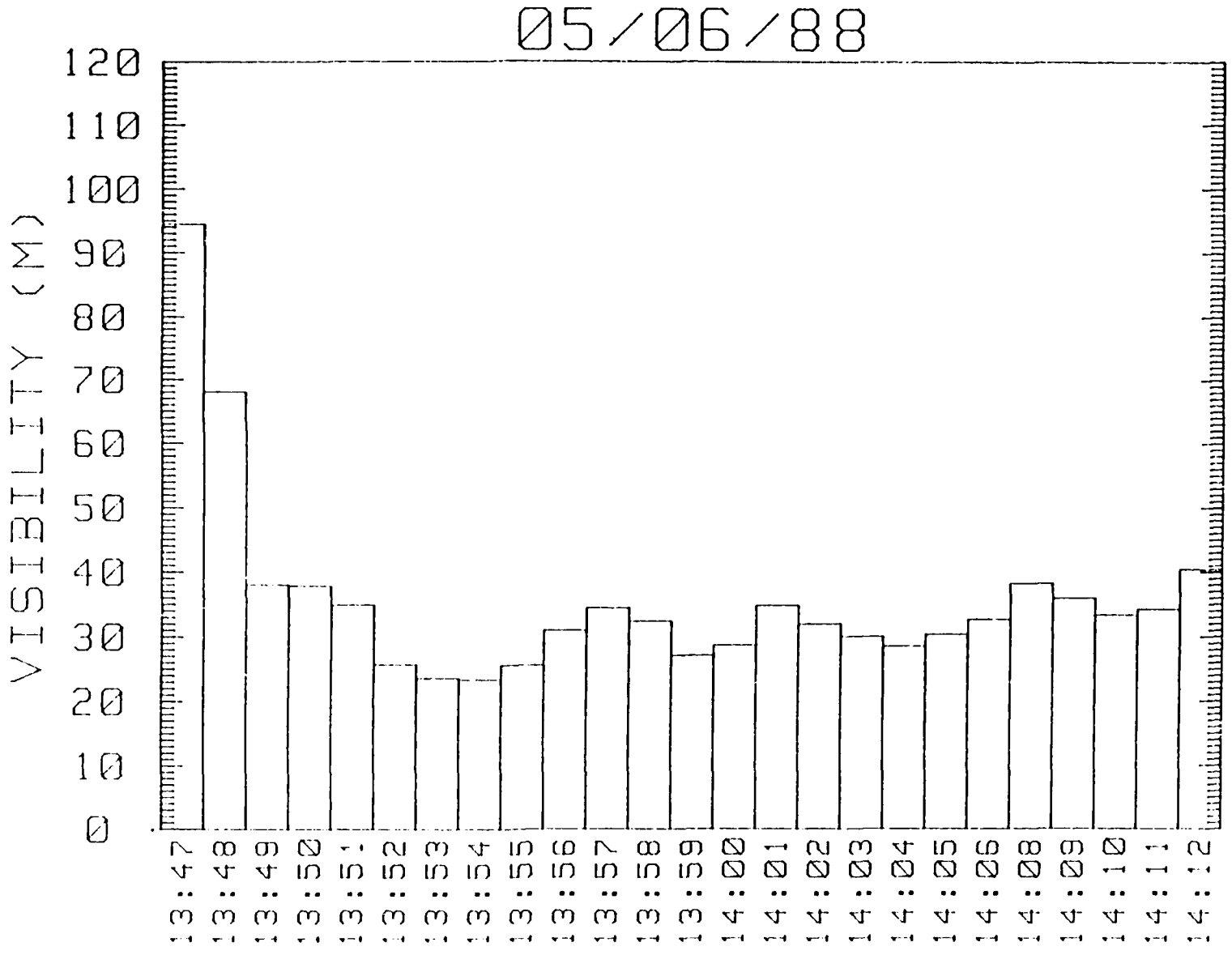

Fig. 8 Visibility during the first ice fog test.

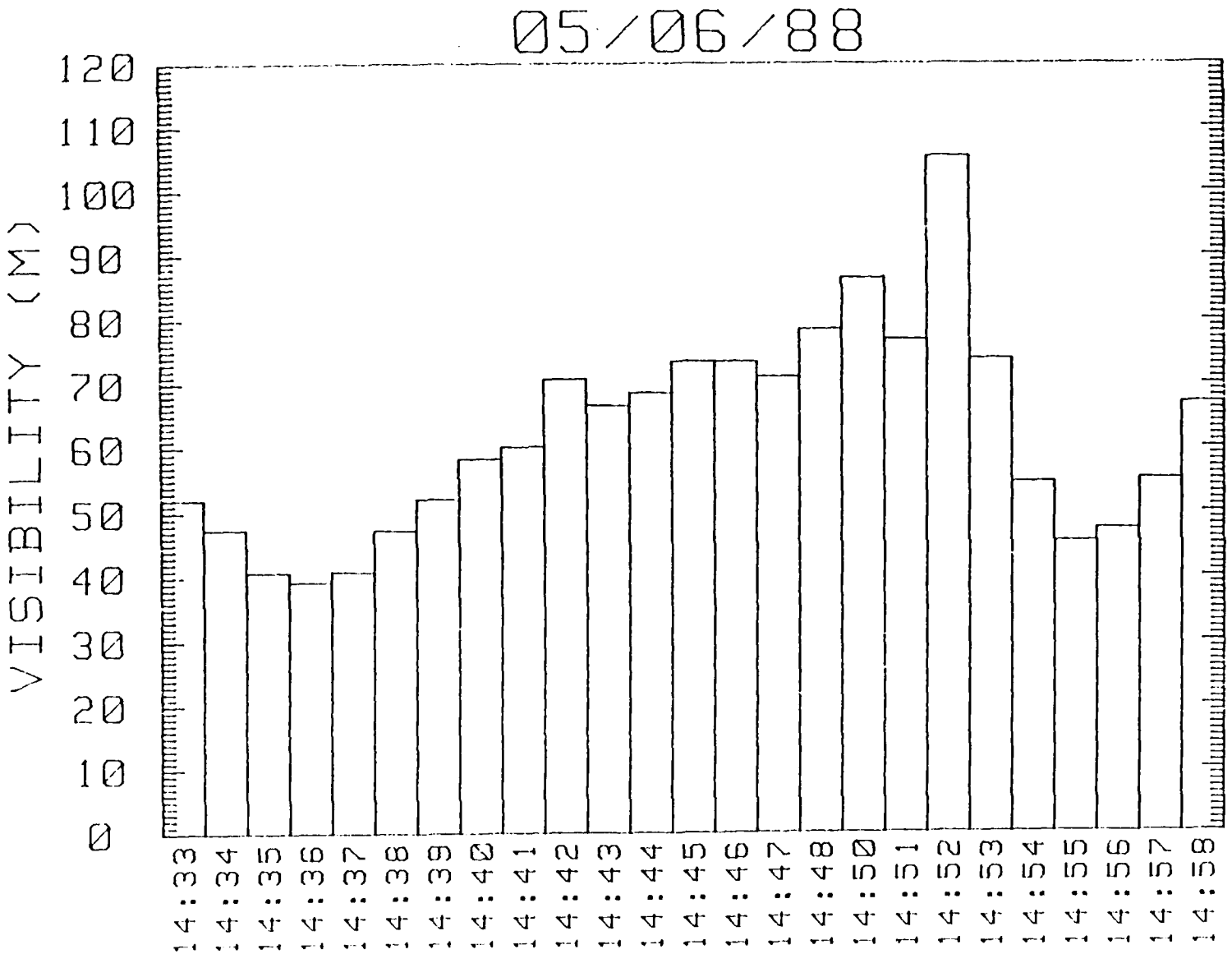

Fig. 9 Visibility during the second ice fog test.

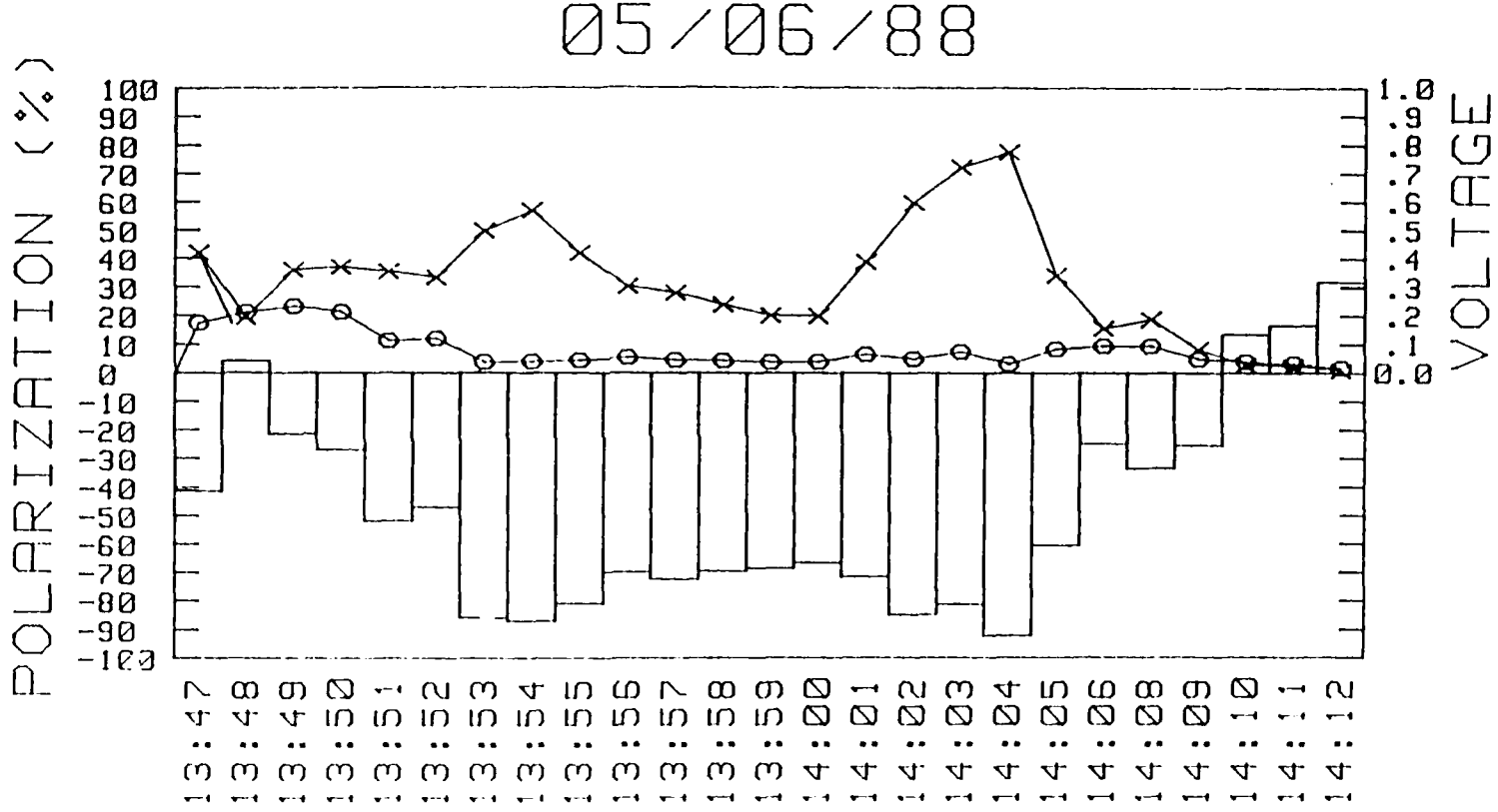

Fig. 10 — Polarization data from the first ice fog.

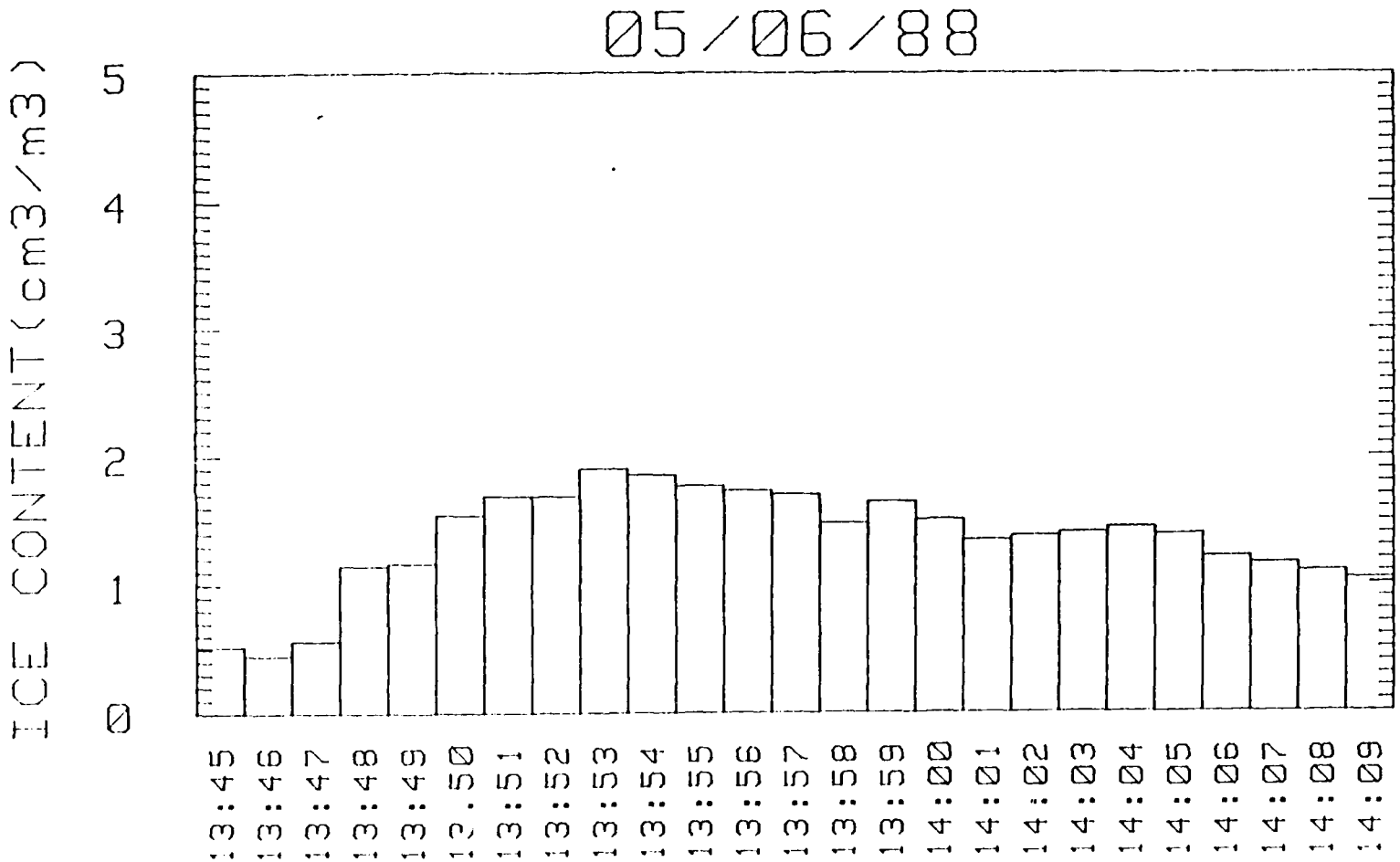

Fig. 11 Ice contents computed from size distributions.

Fig. 12 Ice content computed from size distributions.

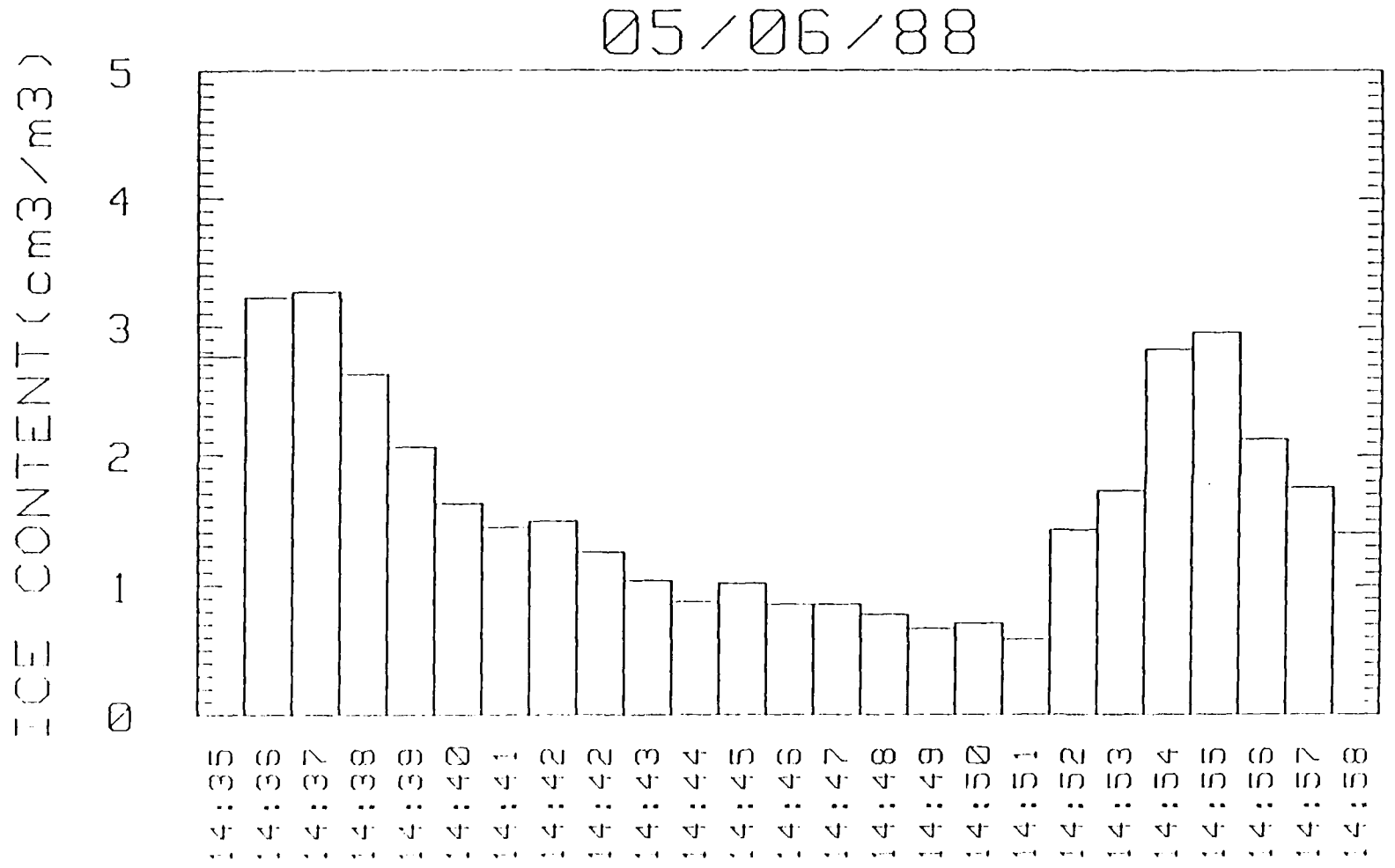

Fig. 13 Ice content computed from size distributions.

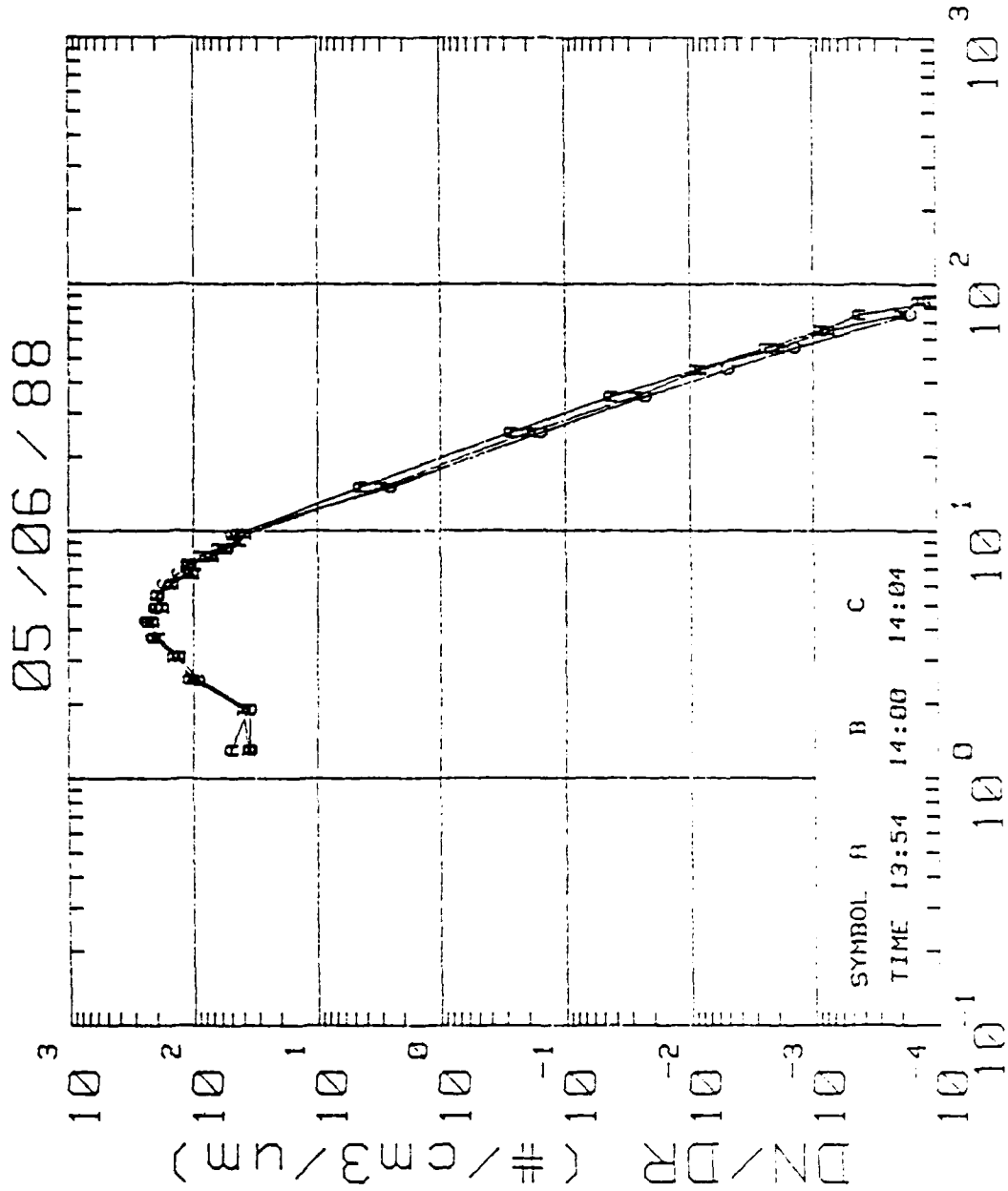

Fig. 14 Size distributions obtained during the ice fogs.

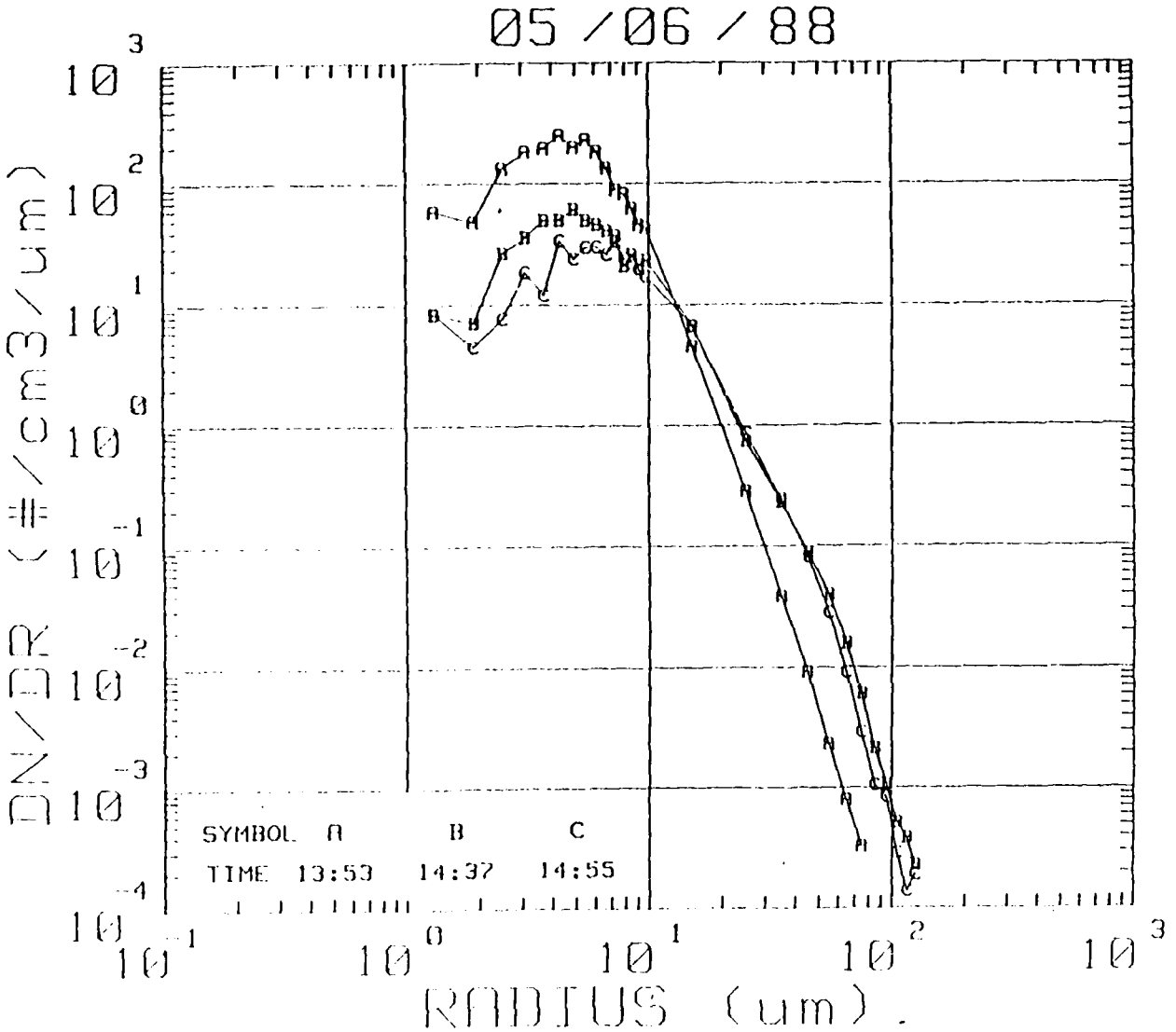

Fig. 15 Size distributions from the three ice fogs.

50 lbs/s. The first injection started at 0943, lasted for 7 min. and produced a thin ice fog (VR=500m). A second injection started at 1002 and lasted for 9 min., the chamber warmed to about -3°C, no ice was observed and a VR of 20 m was obtained. A third injection starting at 1035 and lasting 9 minutes yielded a VR of 14 m, while the fourth injection (15 min.) starting at 1120, accompanied by the burning of newspaper to provide additional condensation nuclei, resulted in a 10 m VR. At 1302 a 6 min. injection produced a VR of 15m. On May 10 the initial chamber temperature was -6°C and we injected saturated air at 31°C. The first injection (starting a 0810) lasted for 7 min. during which newspapers were burned and a VR of 9 m. was obtained. A second injection began at 0823, lasted for 6 min. and brought the VR down to a minimum of 6m. Figure 16, curves A, B and C give size distributions for the fog at times when the visibility was 15, 20 and 25 m respectively. Figure 17 gives three size distributions, all of which correspond to a visibility of 10 m.

In contrast to the ice fog, the wet fogs produced almost no depolarization, as can be seen in Figs. 18-21. Bar charts of visibility, liquid water content and computed visibility can be found in Appendix B.

III. REMARKS

There were a couple of instances when the HSS visiometer indicated high values for the visual range that did not correspond with visual observations. Due to the time constant incorporated into the instrument it then required several minutes to settle to the proper value. Times at which the HSS data may be erroneous are: 5/4 1052-1058, 5/6 1347-1348 and 1430-1432. The two times on 5/6 appeared to coincide with the operation of the overhead door during chamber humidification.

When the visibility was less than about 9 m there were too many particles for the PMS CSAS to properly size and count. This results in erroneous LWCs and computed VRs during these times. In addition, there are several obvious discontinuities in the LWC and computed VR data which are not physically possible; if values at these specific times are required, smoothing using the neighboring data should be used to obtain representative values.

IV. ACKNOWLEDGEMENTS

The authors would like to thank Dr. Hermann Gerber for his expert assistance on the design of the polarization instrument.

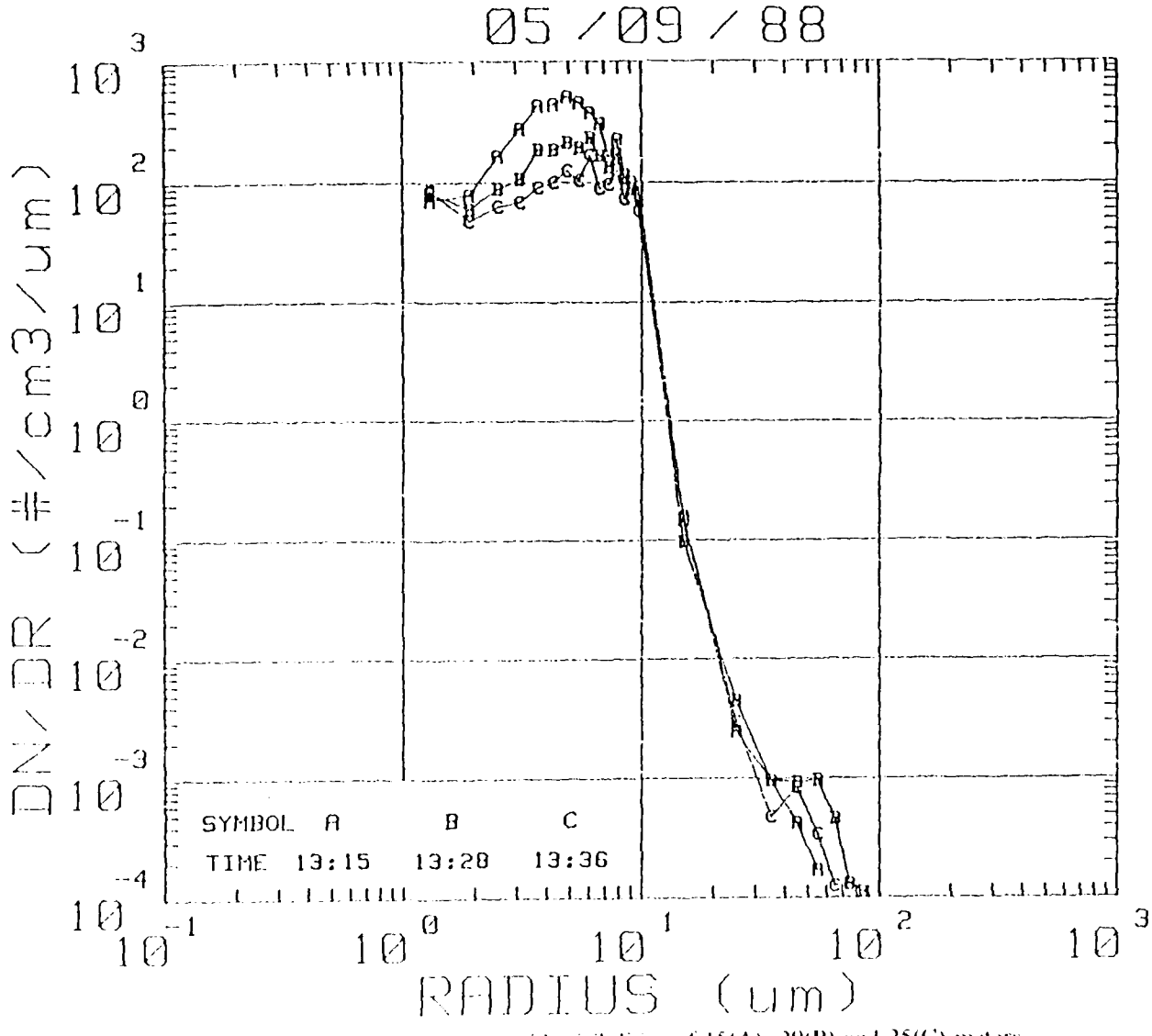

Fig. 16 Size distributions for wet fogs with visibilities of 15(A), 20(B) and 25(C) meters.

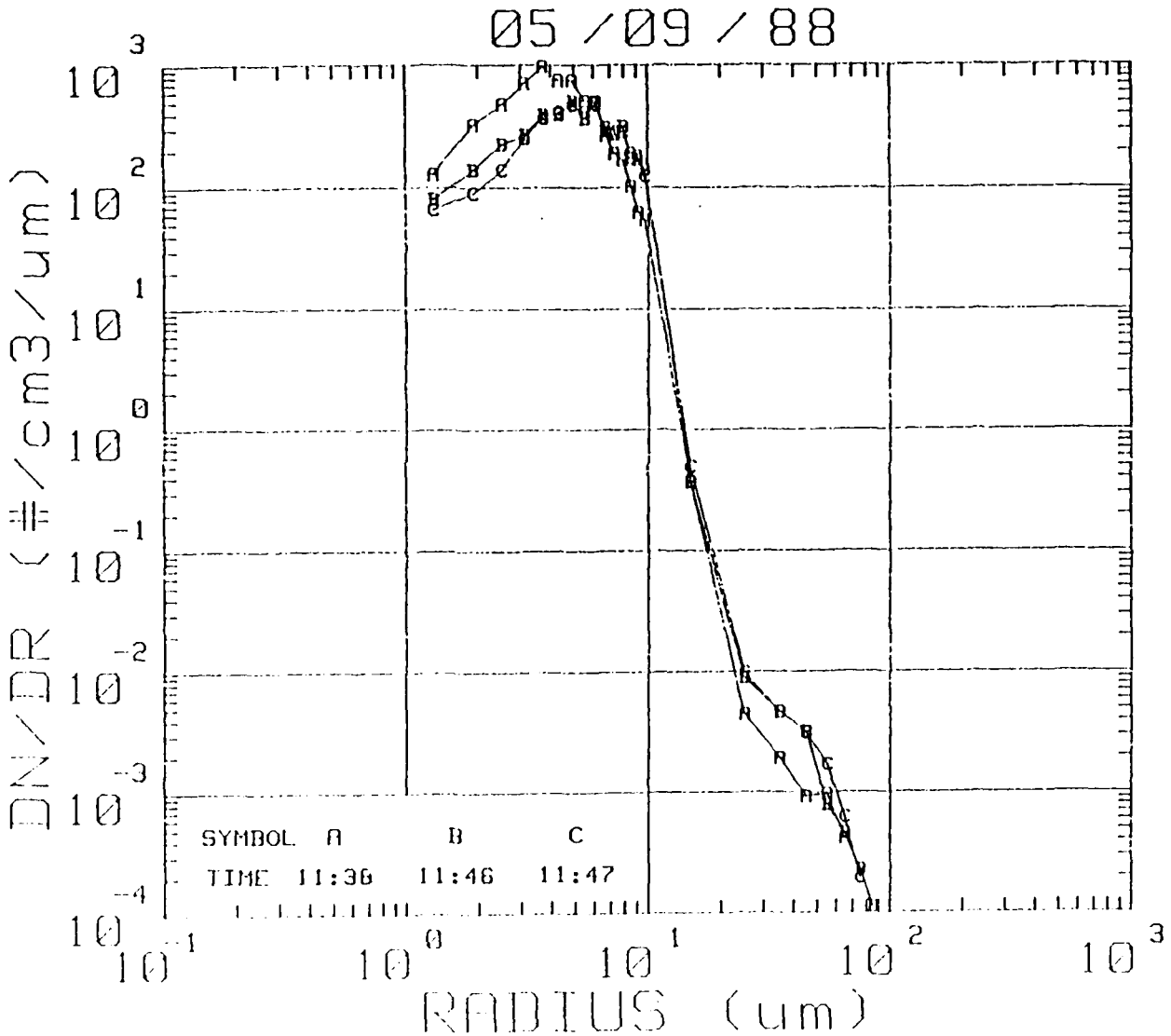

Fig. 17 Size distributions for wet fogs with a visibility of 10 meters.

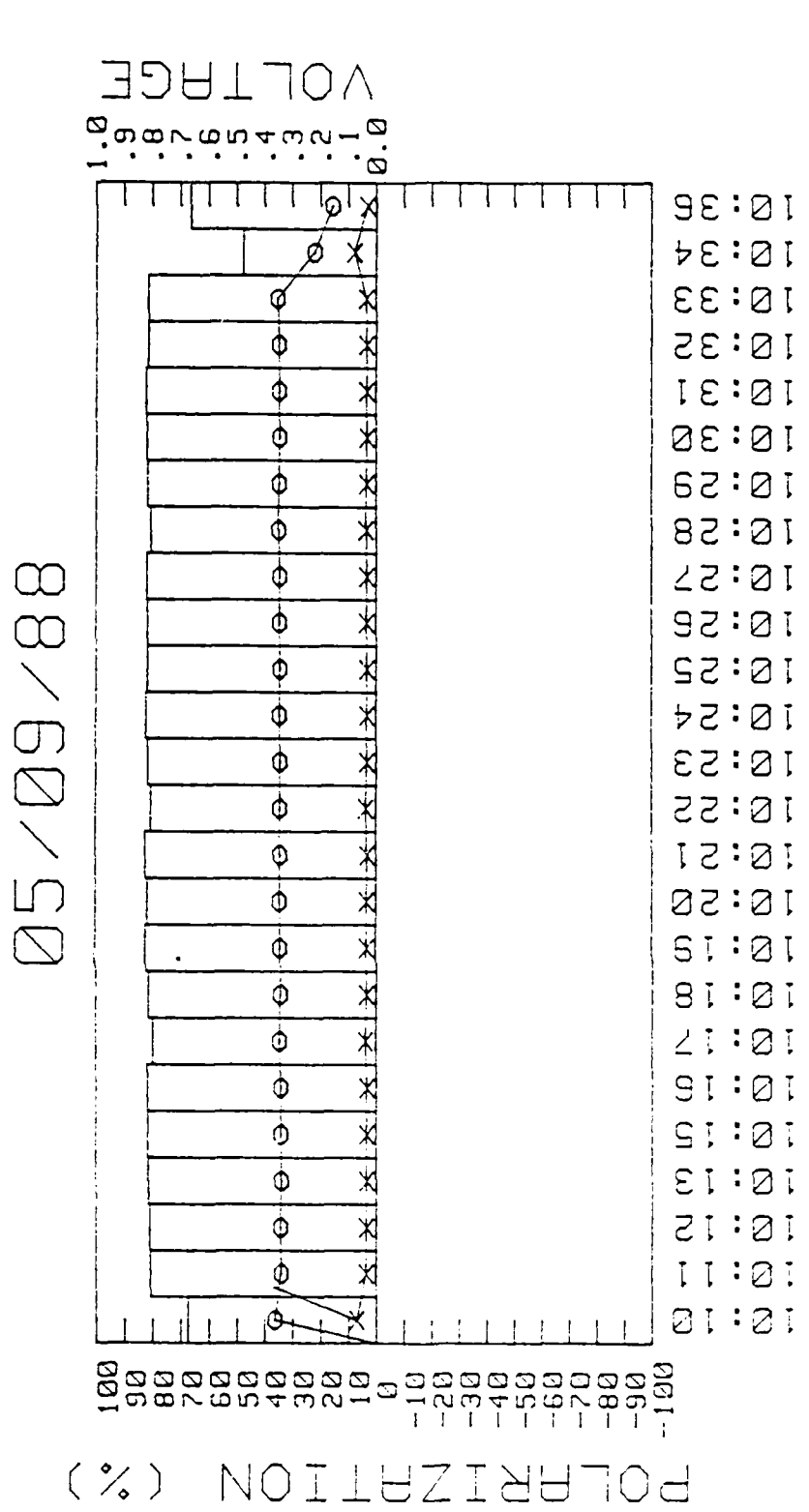

Fig. 18 - Polarization data from a wet fog.

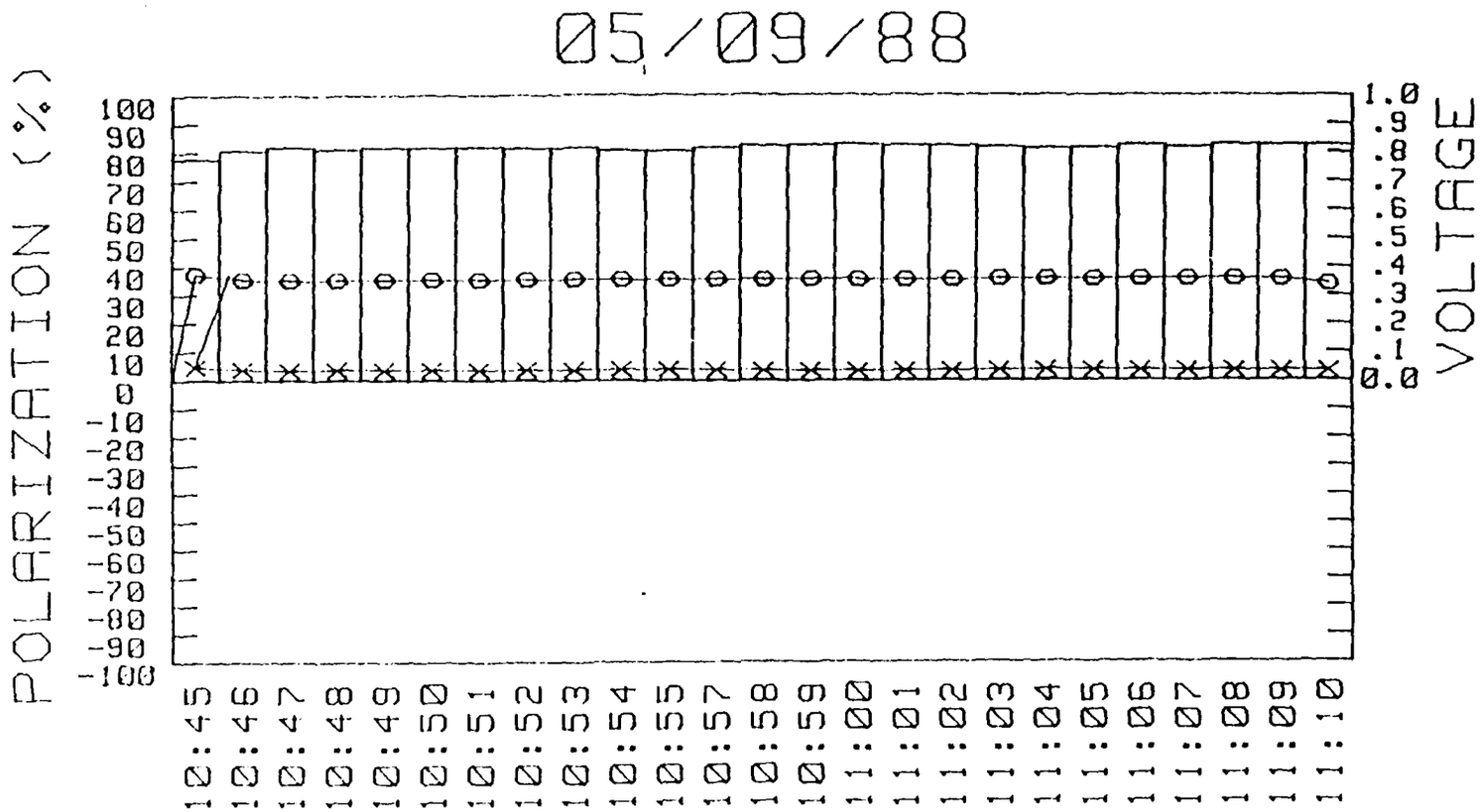

Fig. 19 — Polarization data from a wet fog.

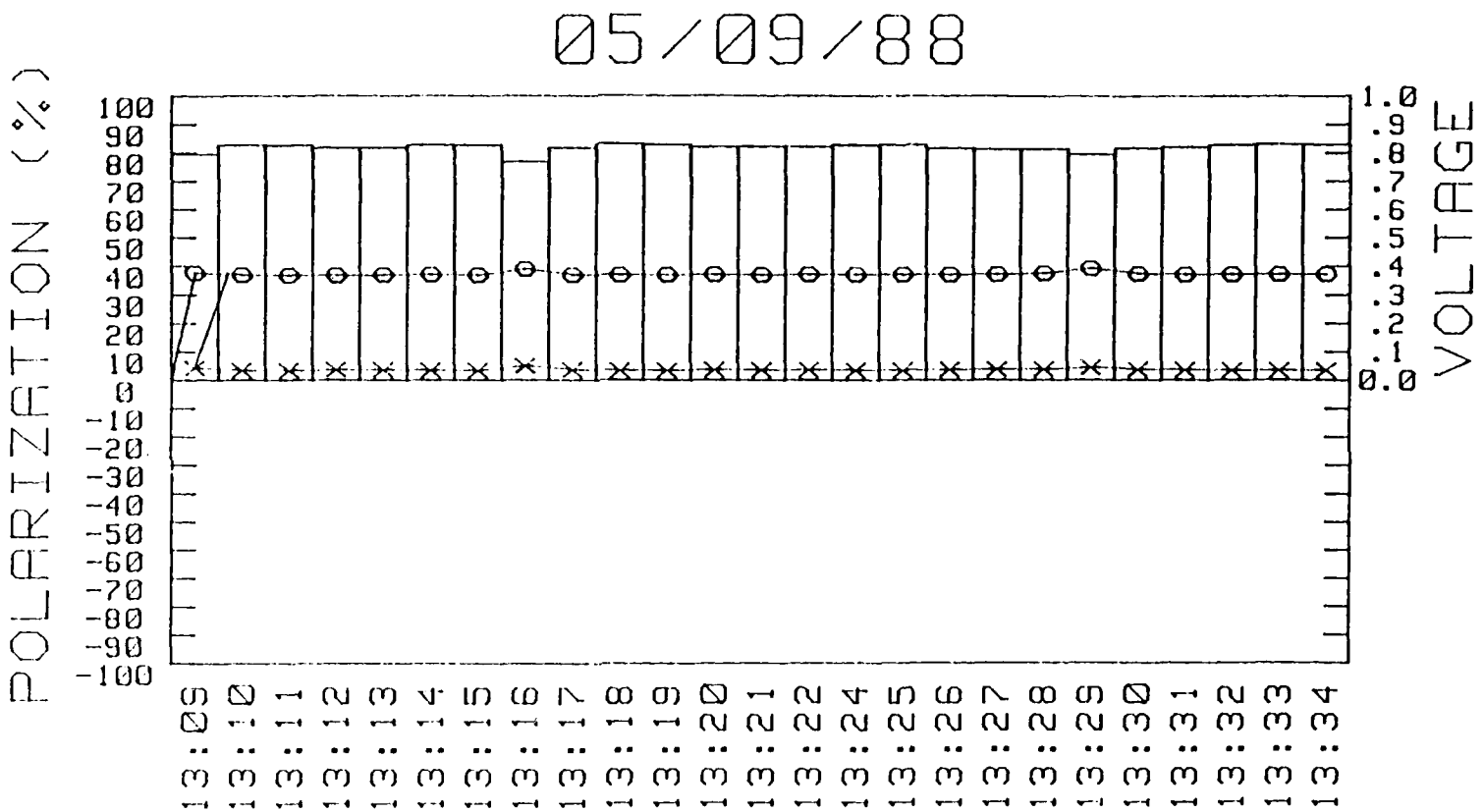

Fig. 20 — Polarization data from a wet fog.

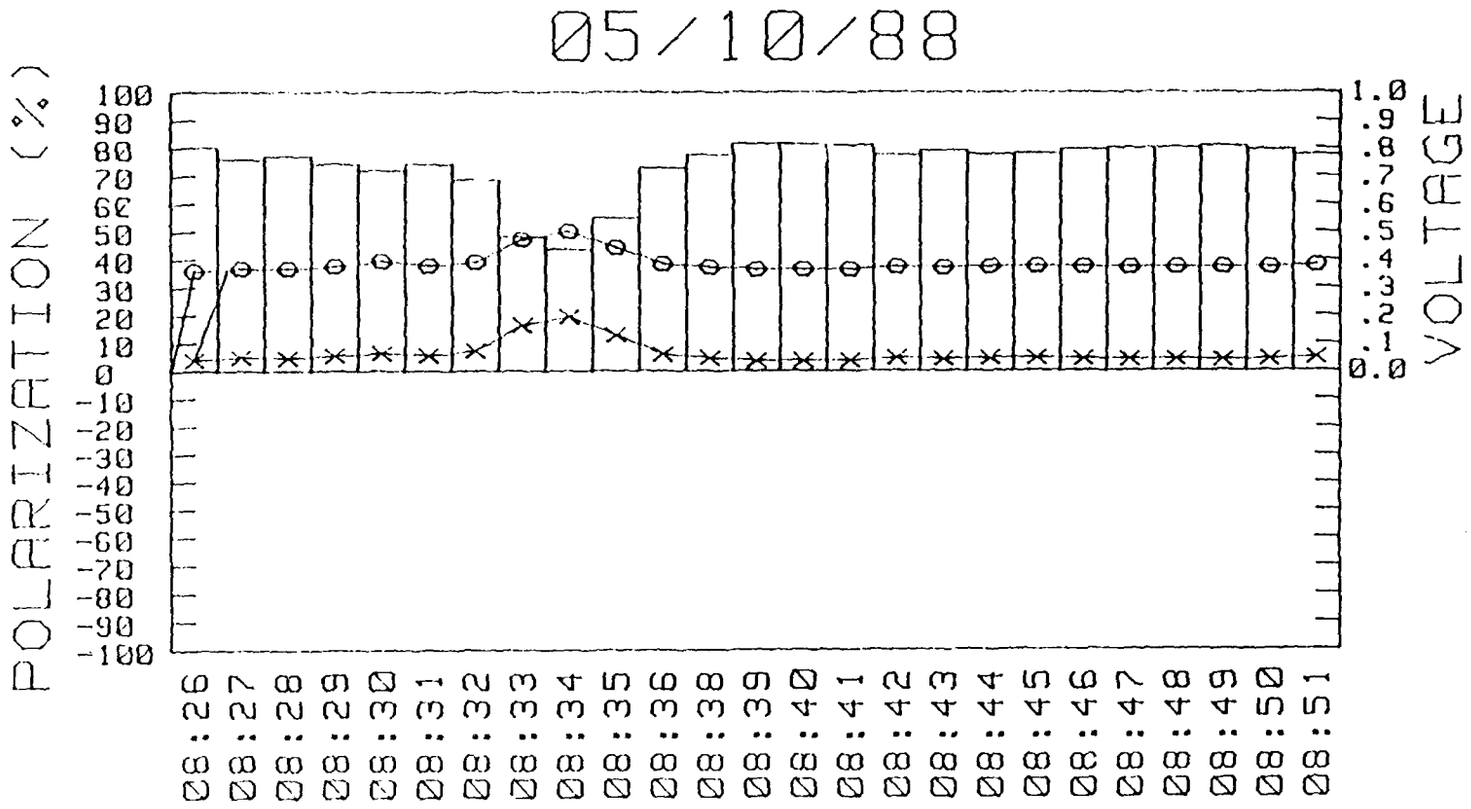

Fig. 21 - Polarization data from a wet fog.

Appendix A.

The following measurements of the visual range were obtained with the HSS visiometer during the rain tests.

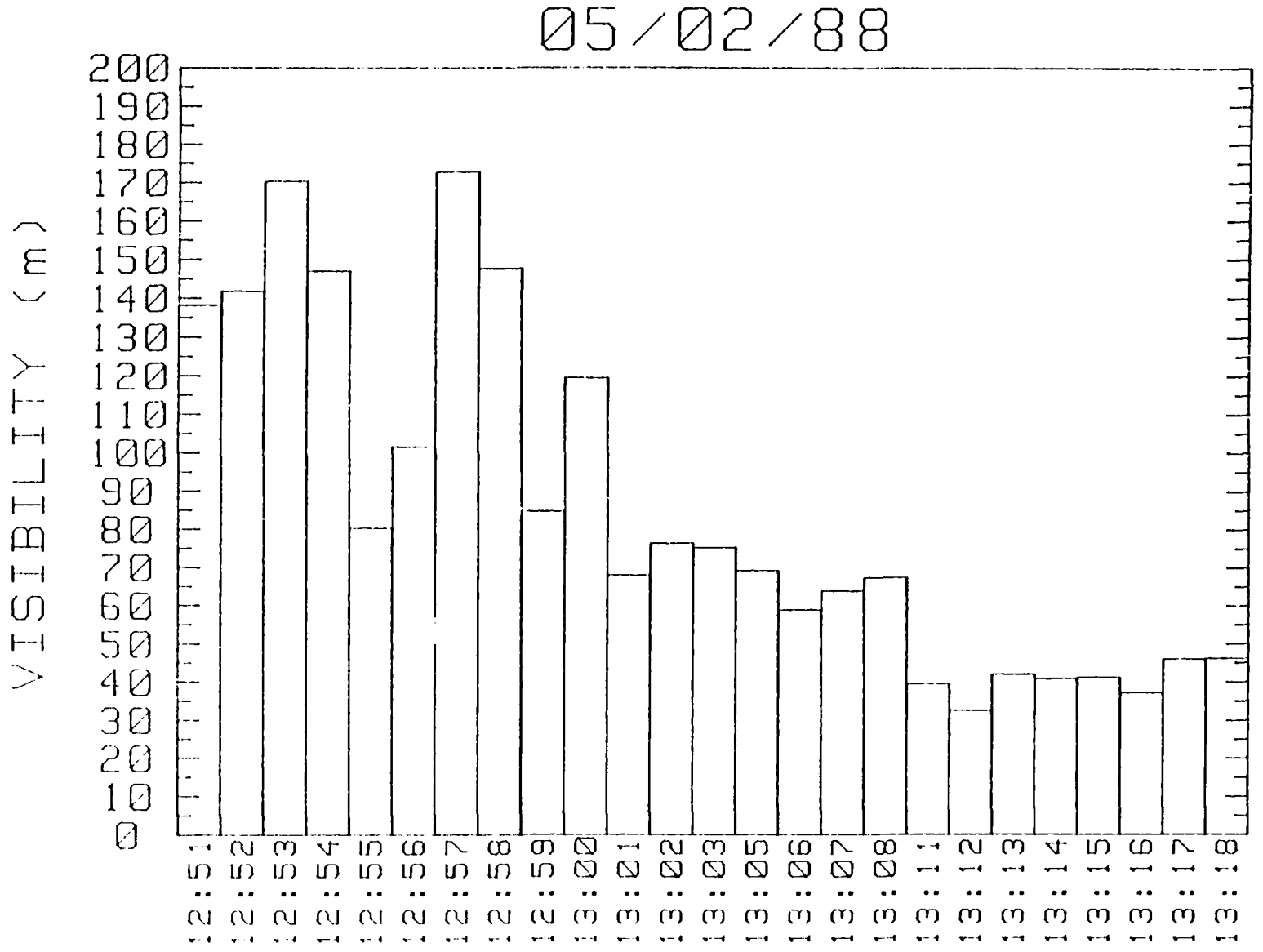
05/02/88
VISIBILITY (m)
200
190
180
170
160
150
140
130
120
110
100
90
80
70
60
50
40
30
20
10
0
12:51
12:52
12:53
12:54
12:55
12:56
12:57
12:58
12:59
13:00
13:01
13:02
13:03
13:05
13:06
13:07
13:08
13:11
13:12
13:13
13:14
13:15
13:16
13:17
13:18

05/02/88
VISIBILITY (m)
200
190
180
170
160
150
140
130
120
110
100
90
80
70
60
50
40
30
20
10
0
13:19
13:20
13:21
13:22
13:23
13:24
13:25
13:26
13:27
13:28
13:29
13:30
13:32
13:33
13:34
13:35
13:36
13:37
13:38
13:39
13:40
13:41
13:43
13:44
13:45

05/02/88
VISIBILITY (m)
0
100
200
300
400
500
600
700
800
900
1000
1100
1200
1300
1400
1500
1600
1700
1800
1900
2000
13:48
13:49
13:50
13:51
13:52
13:53
13:54
13:55
13:56
13:57
13:58
13:59
14:00
14:01
14:02
14:03
14:04
14:05
14:06
14:07
14:12
14:13
14:14
14:15
14:16

05/03/88
VISIBILITY (m)
0
10
20
30
40
50
60
70
80
90
100
110
120
130
140
150
160
170
180
190
200
08:25
08:26
08:27
08:28
08:29
08:30
08:31
08:32
08:33
08:34
08:35
08:37
08:38
08:39
08:40
08:41
08:42
08:43
08:44
08:45
08:46
08:47
08:48
08:49
08:50

05/03/88
08:51
08:52
08:53
08:54
08:55
08:57
08:58
08:59
09:00
09:01
09:02
09:03
09:04
09:05
09:06
09:07
09:08
09:09
09:10
09:11
09:12
09:13
09:14
09:15
09:16
0
10
20
30
40
50
60
70
80
90
100
110
120
130
140
150
160
170
180
190
200
VISIBILITY (m)

05/03/88
09:45
09:44
09:43
09:42
09:39
09:37
09:36
09:35
09:34
09:33
09:32
09:31
09:30
09:29
09:28
09:27
09:26
09:25
09:24
09:23
09:22
09:21
09:20
09:19
09:18
200
190
180
170
160
150
140
130
120
110
100
90
80
70
60
50
40
30
20
10
0
VISIBILITY (m)

05/03/88
09:52
09:51
09:50
09:49
09:48
09:47
09:46
09:45
09:44
09:43
09:42
09:39
09:37
09:36
09:35
09:34
09:33
09:32
09:31
09:30
09:29
09:28
09:27
09:26
09:25
200
190
180
170
160
150
140
130
120
110
100
90
80
70
60
50
40
30
20
10
0
VISIBILITY (m)

05/04/88
VISIBILITY (m)
0
10
20
30
40
50
60
70
80
90
100
110
120
130
140
150
160
170
180
190
200
04:00
05:00
06:00
07:00
08:00
09:00
10:00
11:00
12:00
13:00
14:00
15:00
16:00
17:00
18:00
19:00
20:00
21:00
22:00
23:00
24:00
25:00
26:00
27:00
28:00
29:00

05/04/88
VISIBILITY (m)
0
10
20
30
40
50
60
70
80
90
100
110
120
130
140
150
160
170
180
190
200
09:30
09:31
09:32
09:33
09:34
09:35
09:37
09:38
09:39
09:40
09:41
09:42
09:43
09:44
09:45
09:46
09:47
09:48
09:49
09:50
09:51
09:52
09:53
09:54
09:55

05/04/88
VISIBILITY (m)
0
10
20
30
40
50
60
70
80
90
100
110
120
130
140
150
160
170
180
190
200
09:57
09:58
09:59
10:00
10:01
10:02
10:03
10:04
10:05
10:06
10:07
10:08
10:09
10:10
10:11
10:12
10:13
10:14
10:15
10:16
10:18
10:19
10:20
10:21
10:22

05/04/88
10:23
10:24
10:25
10:26
10:27
10:28
10:29
10:30
10:31
10:32
10:33
10:34
10:35
10:35
10:37
10:39
10:40
10:41
10:42
10:43
10:44
10:45
10:46
10:47
10:48
0
10
20
30
40
50
60
70
80
90
100
110
120
130
140
150
160
170
180
190
200
VISIBILITY (m)

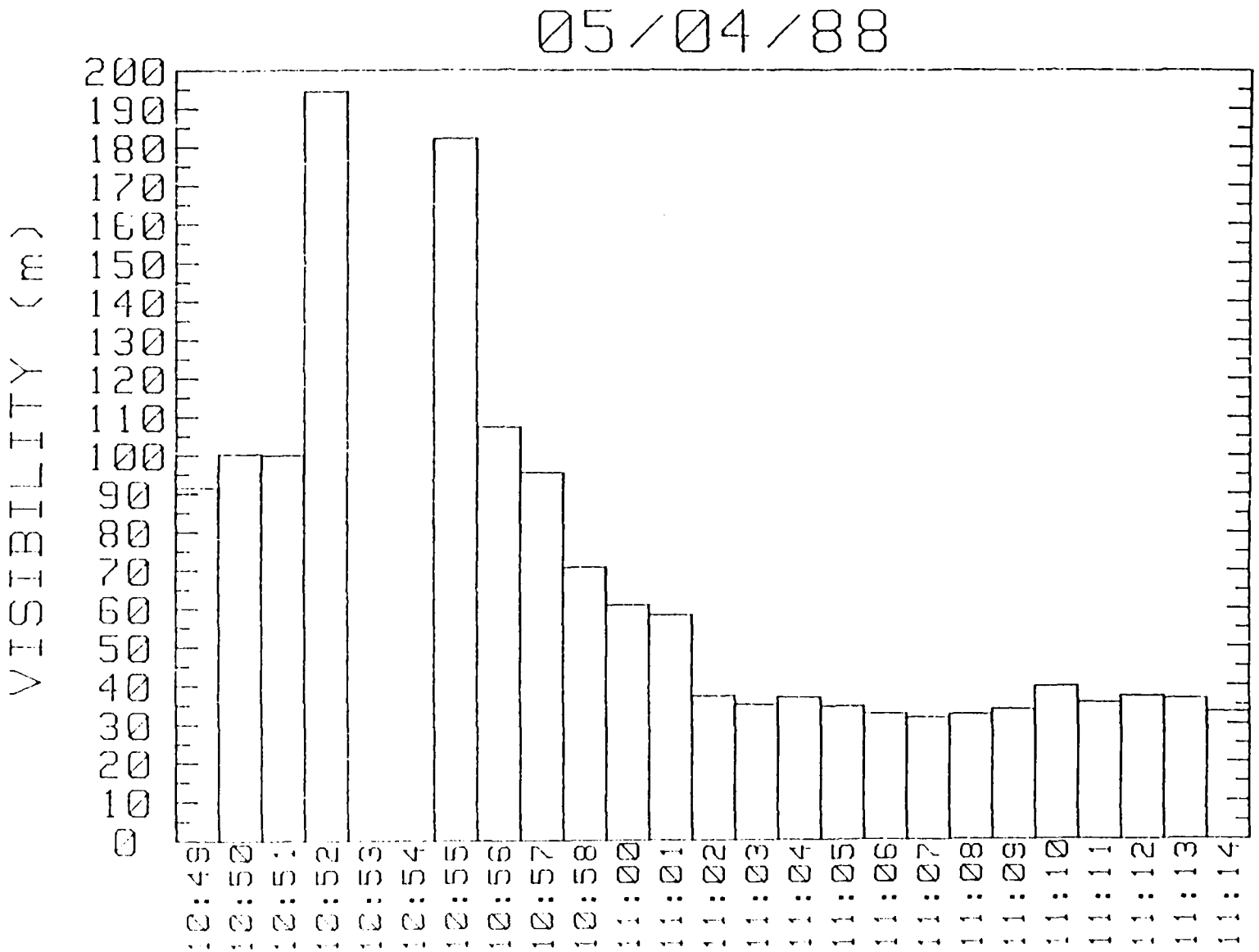
05/04/88
VISIBILITY (m)
200
190
180
170
160
150
140
130
120
110
100
90
80
70
60
50
40
30
20
10
0

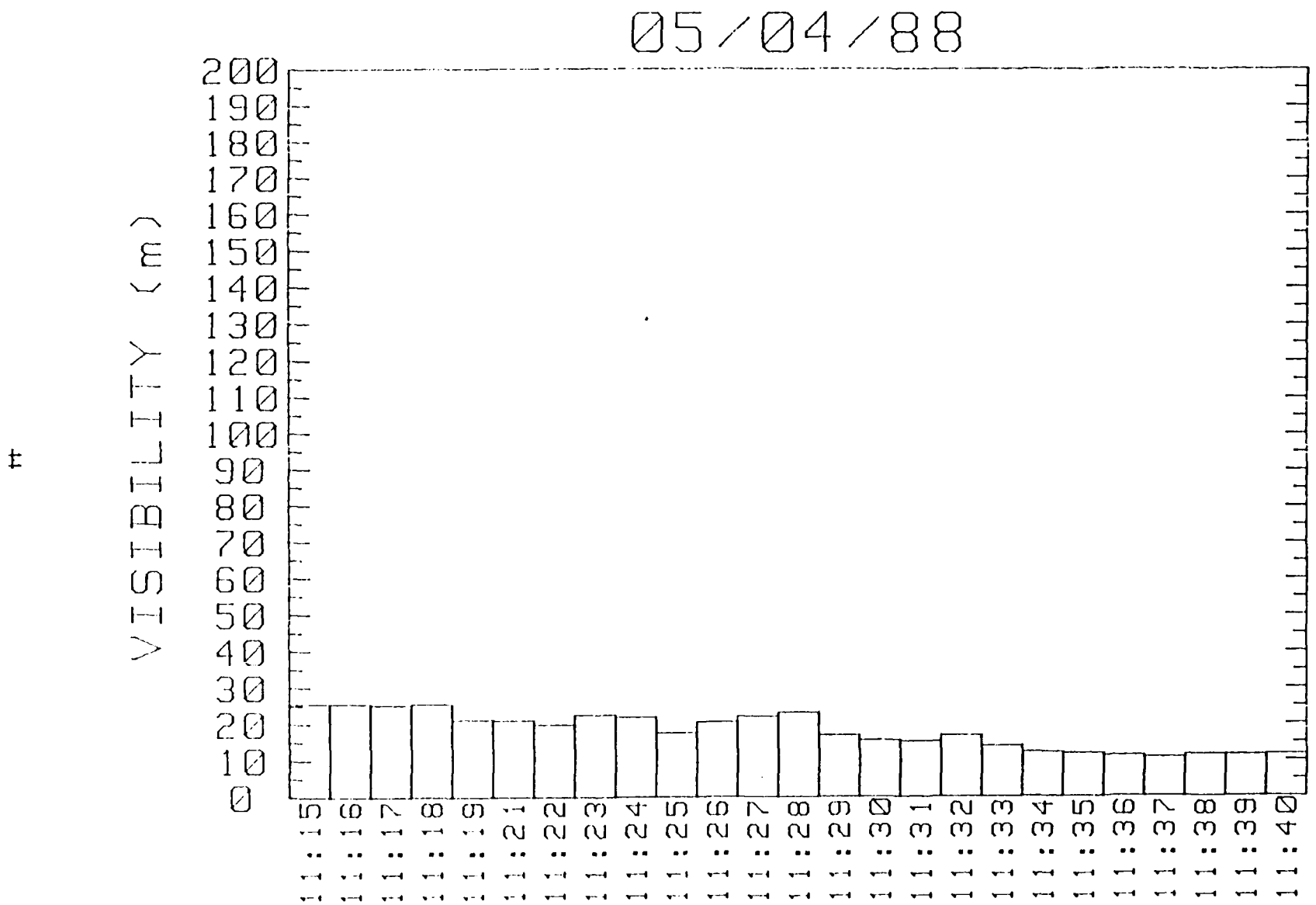
05/04/88
VISIBILITY (m)
200
190
180
170
160
150
140
130
120
110
100
90
80
70
60
50
40
30
20
10
0
11:15
11:16
11:17
11:18
11:19
11:21
11:22
11:23
11:24
11:25
11:26
11:27
11:28
11:29
11:30
11:31
11:32
11:33
11:34
11:35
11:36
11:37
11:38
11:39
11:40

Appendix B.

The following are measurements of the visual range, obtained with the HSS visiometer, and liquid water contents and visual ranges calculated from the PMS aerosol spectrometer data obtained during the fogs.

05/09/88
VISIBILITY (M)
0
10
20
30
40
50
60
70
80
90
100
110
120
10:10
10:11
10:12
10:13
10:15
10:16
10:17
10:18
10:19
10:20
10:21
10:22
10:23
10:24
10:25
10:26
10:27
10:28
10:29
10:30
10:31
10:32
10:33
10:34
10:36

05/09/88
VISIBILITY (M)
0
10
20
30
40
50
60
70
80
90
100
110
120
10:37
10:38
10:39
10:40
10:41
10:42
10:43
10:44
10:45
10:46
10:47
10:48
10:49
10:50
10:51
10:52
10:53
10:54
10:55
10:57
10:58
10:59
11:00
11:01
11:02

05/09/88
VISIBILITY (M)
120
110
100
90
80
70
60
50
40
30
20
10
0
11:03
11:04
11:05
11:06
11:07
11:08
11:09
11:10
11:11
11:12
11:13
11:14
11:15
11:16
11:18
11:19
11:20
11:21
11:22
11:23
11:24
11:25
11:26
11:27
11:28

05/09/88
VISIBILITY (M)
0
10
20
30
40
50
60
70
80
90
100
110
120
11:29
11:30
11:31
11:32
11:33
11:34
11:35
11:36
11:37
11:39
11:40
11:41
11:42
11:43
11:44
11:45
11:46
11:47
11:48
11:49
11:50
11:51
11:52
11:53
11:54

05/09/88
VISIBILITY (M)
0
10
20
30
40
50
60
70
80
90
100
110
120
13:05
13:07
13:08
13:09
13:10
13:11
13:12
13:13
13:14
13:15
13:16
13:17
13:18
13:19
13:20
13:21
13:22
13:24
13:25
13:26
13:27
13:28
13:29
13:30
13:31

05/10/88
VISIBILITY (M)
0
10
20
30
40
50
60
70
80
90
100
110
120
08:14
08:15
08:17
08:18
08:19
08:20
08:21
08:22
08:23
08:24
08:25
08:26
08:27
08:28
08:29
08:30
08:31
08:32
08:33
08:34
08:35
08:36
08:38
08:39
08:40

05/10/88
VISIBILITY (M)
120
110
100
90
80
70
60
50
40
30
20
10
0
08:41
08:42
08:43
08:44
08:45
08:46
08:47
08:48
08:49
08:50
08:51
08:52
08:53
08:54
08:55
08:56
08:57
08:59
09:00
09:01
09:02
09:03
09:04
09:05
09:06

05/10/88
VISIBILITY (M)
120
110
100
90
80
70
60
50
40
30
20
10
0
09:00
09:01
09:02
09:03
09:04
09:05
09:06
09:07
09:08
09:09
09:10
09:11
09:12
09:13
09:14
09:15
09:16
09:17
09:18
09:20
09:21
09:22
09:23
09:24
09:25
09:26
09:27
09:28
09:29
09:30
09:31

05/06/88
CALCULATED VR (m)
0
10
20
30
40
50
60
70
80
90
100
110
120
13:45
13:46
13:47
13:48
13:49
13:50
13:51
13:52
13:53
13:54
13:55
13:56
13:57
13:58
13:59
14:00
14:01
14:02
14:03
14:04
14:05
14:06
14:07
14:08
14:09

05/06/88
CALCULATED VR (m)
120
110
100
90
80
70
60
50
40
30
20
10
0
14:34
14:33
14:32
14:31
14:30
14:29
14:28
14:27
14:26
14:25
14:24
14:23
14:22
14:21
14:20
14:19
14:18
14:17
14:16
14:15
14:14
14:13
14:12
14:11
14:10

05/06/88
CALCULATED VR (m)
0
10
20
30
40
50
60
70
80
90
100
110
120
14:35
14:36
14:37
14:38
14:39
14:40
14:41
14:42
14:42
14:43
14:44
14:45
14:46
14:47
14:48
14:49
14:50
14:51
14:52
14:53
14:54
14:55
14:56
14:57
14:58

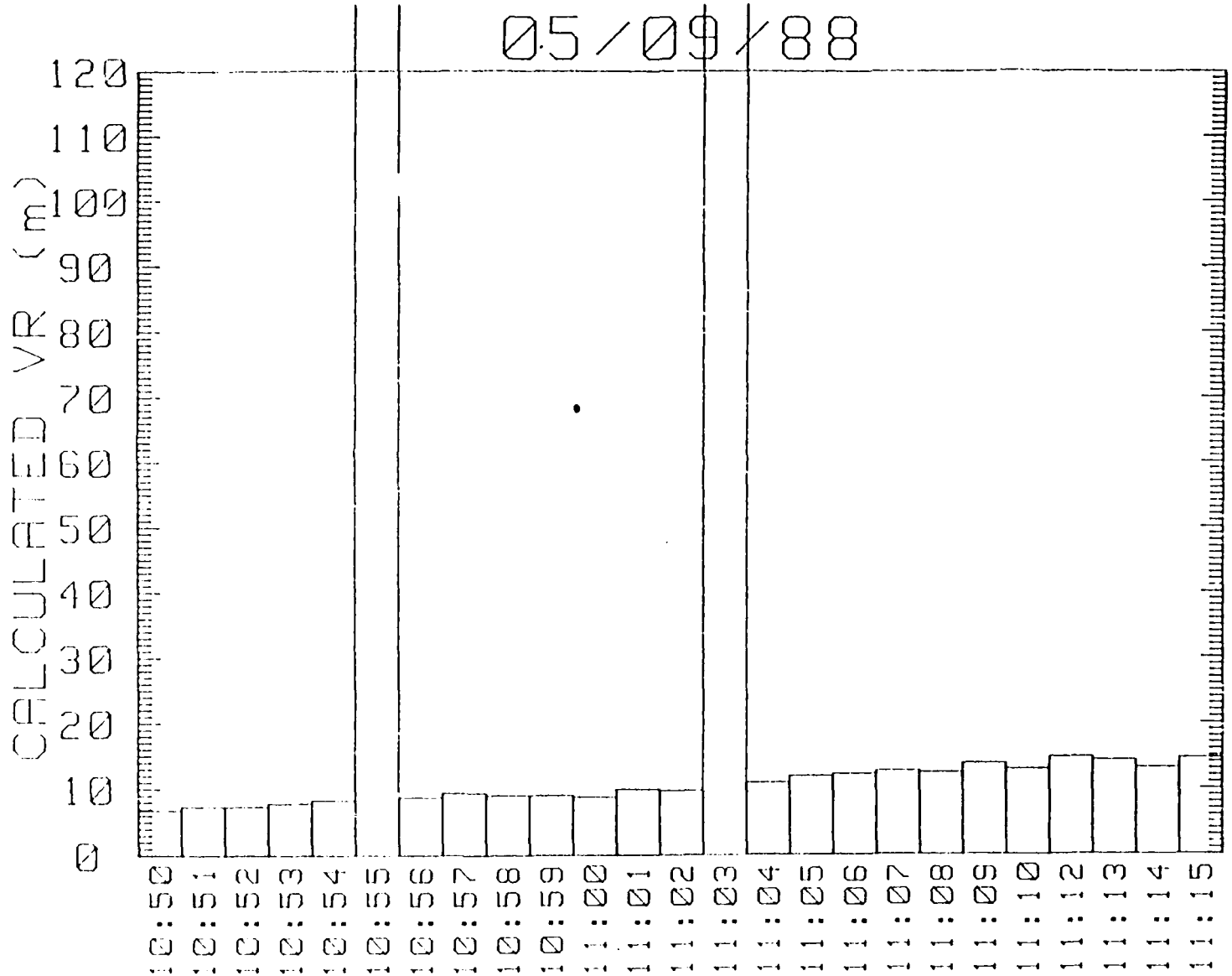
05/09/88
CALCULATED VR (m)
120
110
100
90
80
70
60
50
40
30
20
10
0
10:50
10:51
10:52
10:53
10:54
10:55
10:56
10:57
10:58
10:59
11:00
11:01
11:02
11:03
11:04
11:05
11:06
11:07
11:08
11:09
11:10
11:12
11:13
11:14
11:15

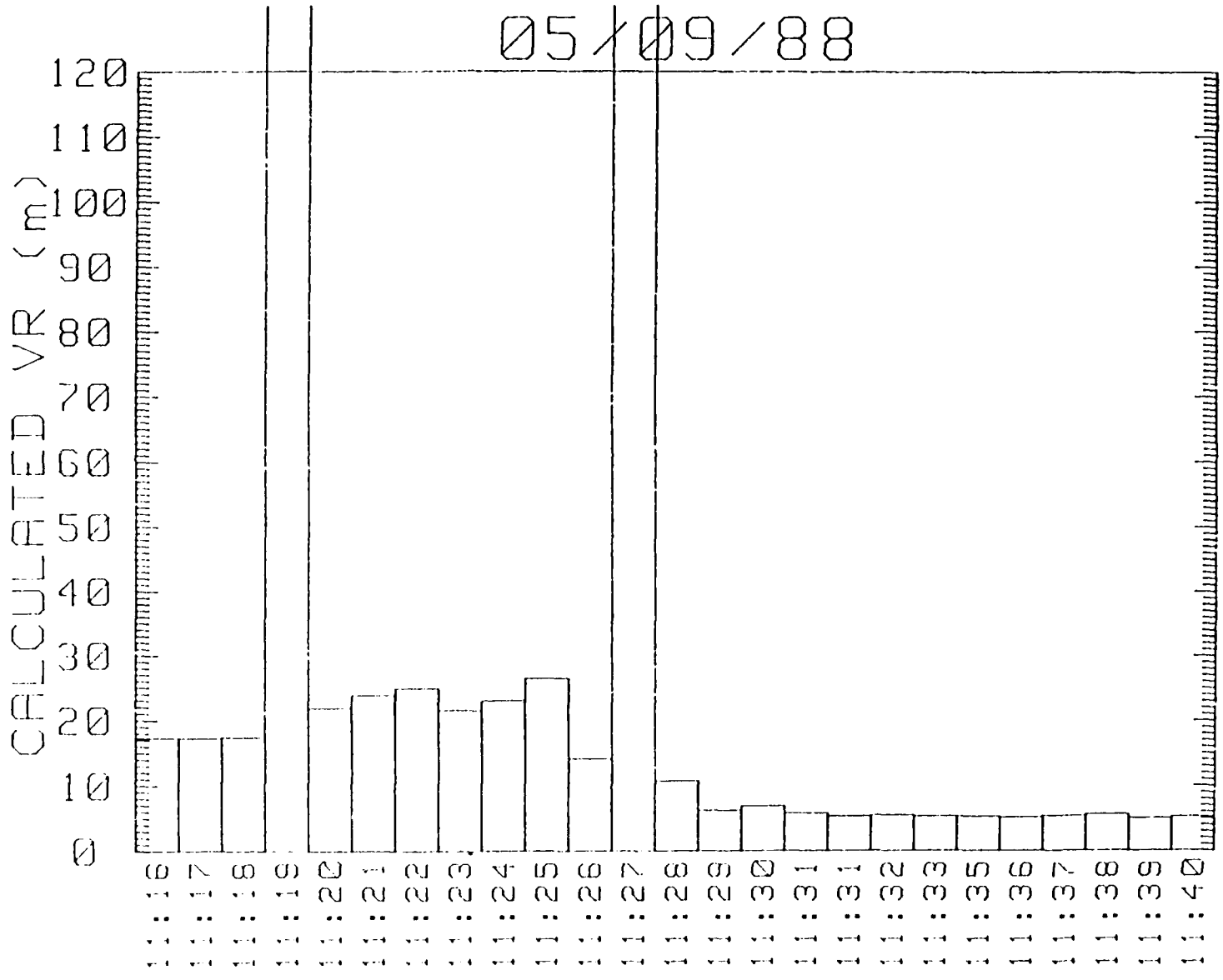
05/09/88
CALCULATED VR (m)
120
110
100
90
80
70
60
50
40
30
20
10
0
16:17:18:19:20:21:22:23:24:25:26:27:28:29:30:31:32:33:34:35:36:37:38:39:40
11 11 11 11 11 11 11 11 11 11 11 11 11 11 11 11 11 11 11 11 11 11 11 11 11

05/09/88
CALCULATED VR (m)
0
10
20
30
40
50
60
70
80
90
100
110
120
11:41
11:42
11:43
11:44
11:45
11:46
11:47
11:48
11:49
11:51
11:52
11:53
11:54
11:55
11:56
11:57
11:58
11:59
12:00
12:02
12:03
12:04
12:04
12:06
12:07

05/09/88
CALCULATED VR (m)
0
10
20
30
40
50
60
70
80
90
100
110
120
13:02
13:01
13:02
13:03
13:04
13:05
13:06
13:07
13:08
13:09
13:10
13:11
13:12
13:13
13:14
13:15
13:16
13:17
13:18
13:19
13:20
13:21
13:22
13:23
13:25
13:26
13:27

05/09/88
13:28
13:29
13:30
13:31
13:32
13:33
13:34
13:35
13:36
13:37
13:38
13:39
13:40
13:41
13:42
13:43
13:44
13:45
13:46
13:48
13:49
13:50
13:51
13:52
13:53
CALCULATED VR (E)
0
10
20
30
40
50
60
70
80
90
100
110
120

05/10/88
08:40
08:39
08:38
08:37
08:36
08:35
08:34
08:33
08:32
08:31
08:30
08:29
08:27
08:26
08:25
08:24
08:23
08:22
08:21
08:19
08:18
08:17
08:16
08:15
08:14
120
110
100
90
80
70
60
50
40
30
20
10
0
CALCULATED VR (m)

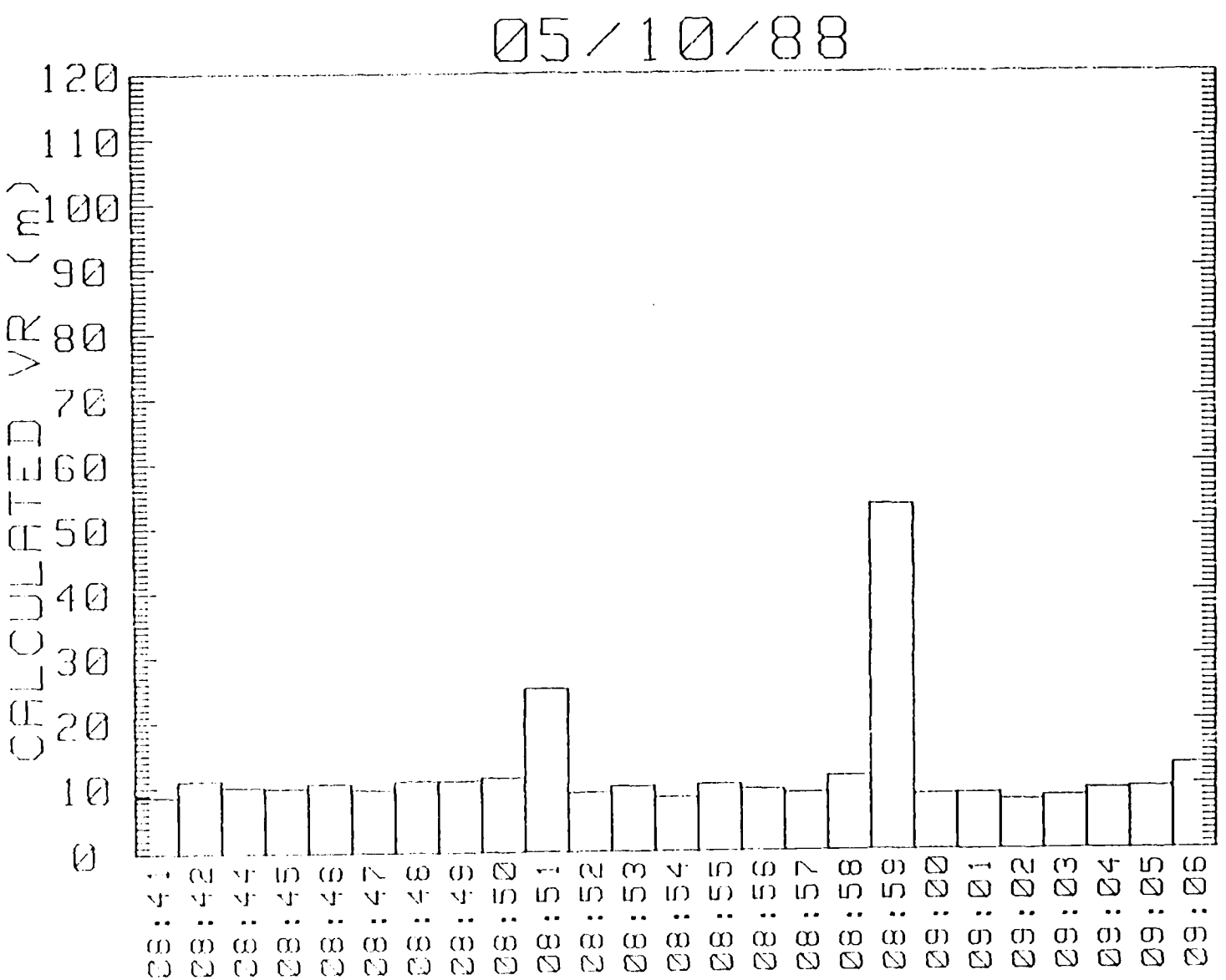
05/10/88
CALCULATED VR (m)
120
110
100
90
80
70
60
50
40
30
20
10
0
08:41
08:42
08:43
08:45
08:46
08:47
08:48
08:49
08:50
08:51
08:52
08:53
08:54
08:55
08:56
08:57
08:58
08:59
09:00
09:01
09:02
09:03
09:04
09:05
09:06

05/10/88
CALCULATED VR (m)
120
110
100
90
80
70
60
50
40
30
20
10
0
09:32
09:31
09:30
09:29
09:28
09:27
09:26
09:25
09:24
09:23
09:21
09:22
09:19
09:18
09:17
09:16
09:15
09:13
09:12
09:11
09:10
09:09
09:08
09:07
09:06

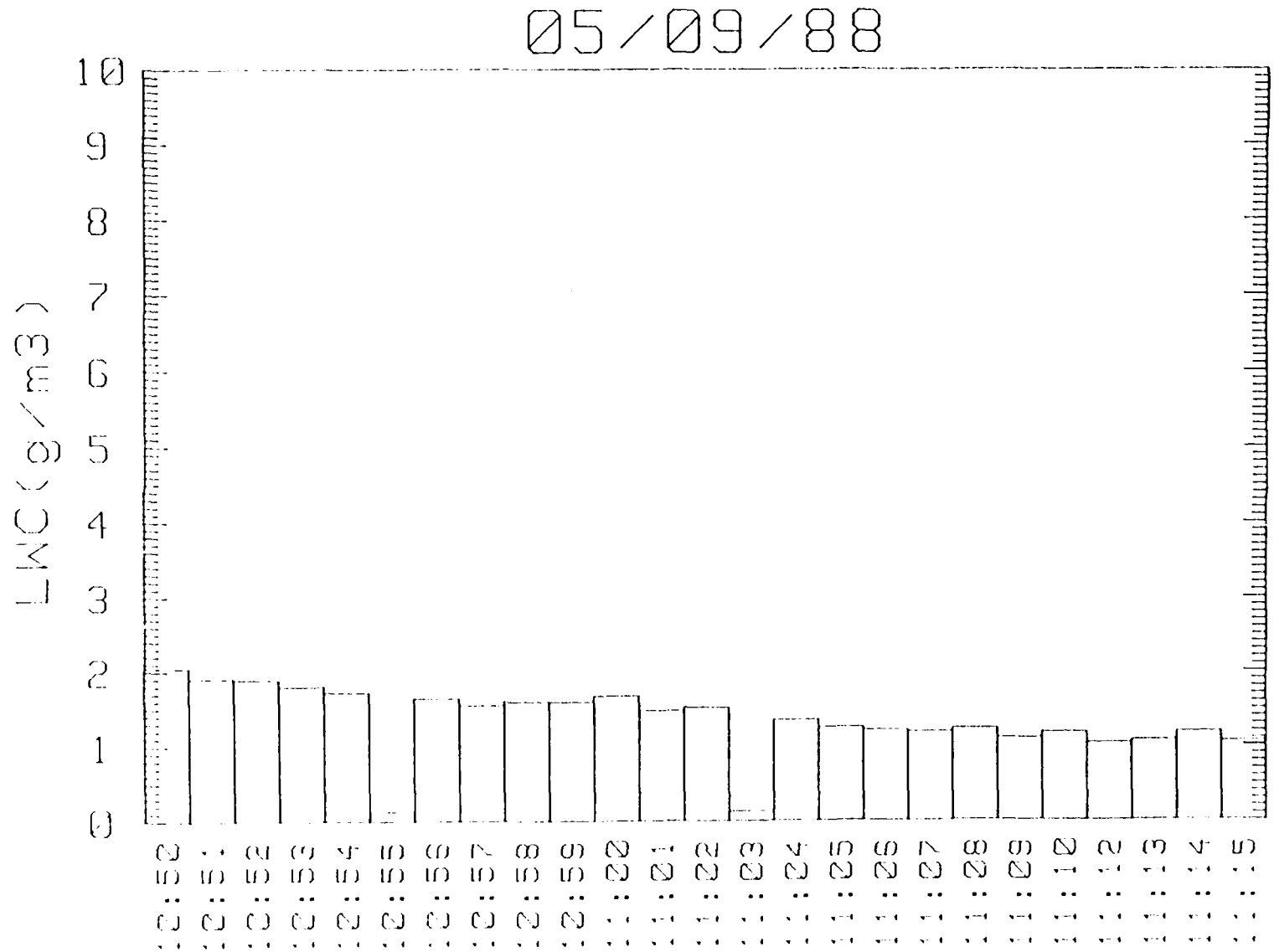
05/09/88
LWC (g/m3)
10
9
8
7
6
5
4
3
2
1
0

05/09/88
LWC (g/m3)
0
1
2
3
4
5
6
7
8
9
10
11:17
11:18
11:19
11:20
11:21
11:22
11:23
11:24
11:25
11:26
11:27
11:28
11:29
11:30
11:31
11:32
11:33
11:35
11:36
11:37
11:38
11:39
11:40

05/09/88
LWC (g/m3)
0
1
2
3
4
5
6
7
8
9
10
12:27
12:26
12:25
12:24
12:23
12:22
12:21
12:20
11:59
11:58
11:57
11:56
11:55
11:54
11:53
11:52
11:51
11:50
11:49
11:48
11:47
11:46
11:45
11:44
11:43
11:42
11:41
11:40

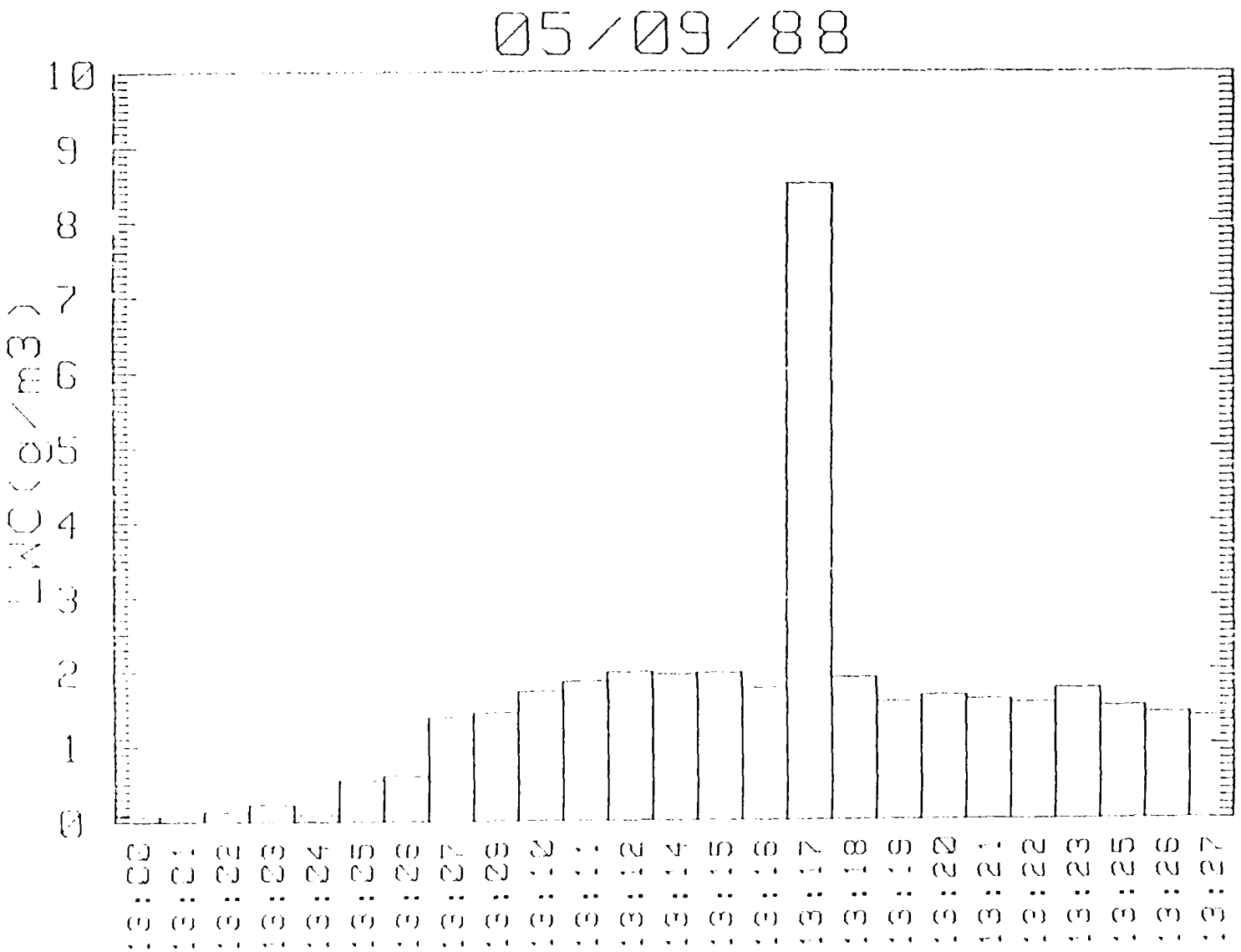
05/09/88
10
9
8
7
6
5
4
3
2
1
0

05/09/88
LWC (g/m3)
0
1
2
3
4
5
6
7
8
9
10
13:28
13:29
13:32
13:31
13:32
13:33
13:34
13:35
13:36
13:37
13:38
13:39
13:40
13:41
13:42
13:43
13:44
13:45
13:46
13:48
13:49
13:50
13:51
13:52
13:53

05/10/88
LWC(g/m3)
0
1
2
3
4
5
6
7
8
9
10
08:14
08:15
08:16
08:17
08:18
08:19
08:21
08:22
08:23
08:24
08:25
08:26
08:27
08:29
08:30
08:31
08:32
08:33
08:34
08:35
08:36
08:37
08:38
08:39
08:40

05/10/88
LWC (g/m3)
0
1
2
3
4
5
6
7
8
9
10
08:41
08:43
08:44
08:45
08:46
08:47
08:48
08:49
08:50
08:51
08:52
08:53
08:54
08:55
08:56
08:57
08:58
08:59
09:00
09:01
09:02
09:03
09:04
09:05
09:06

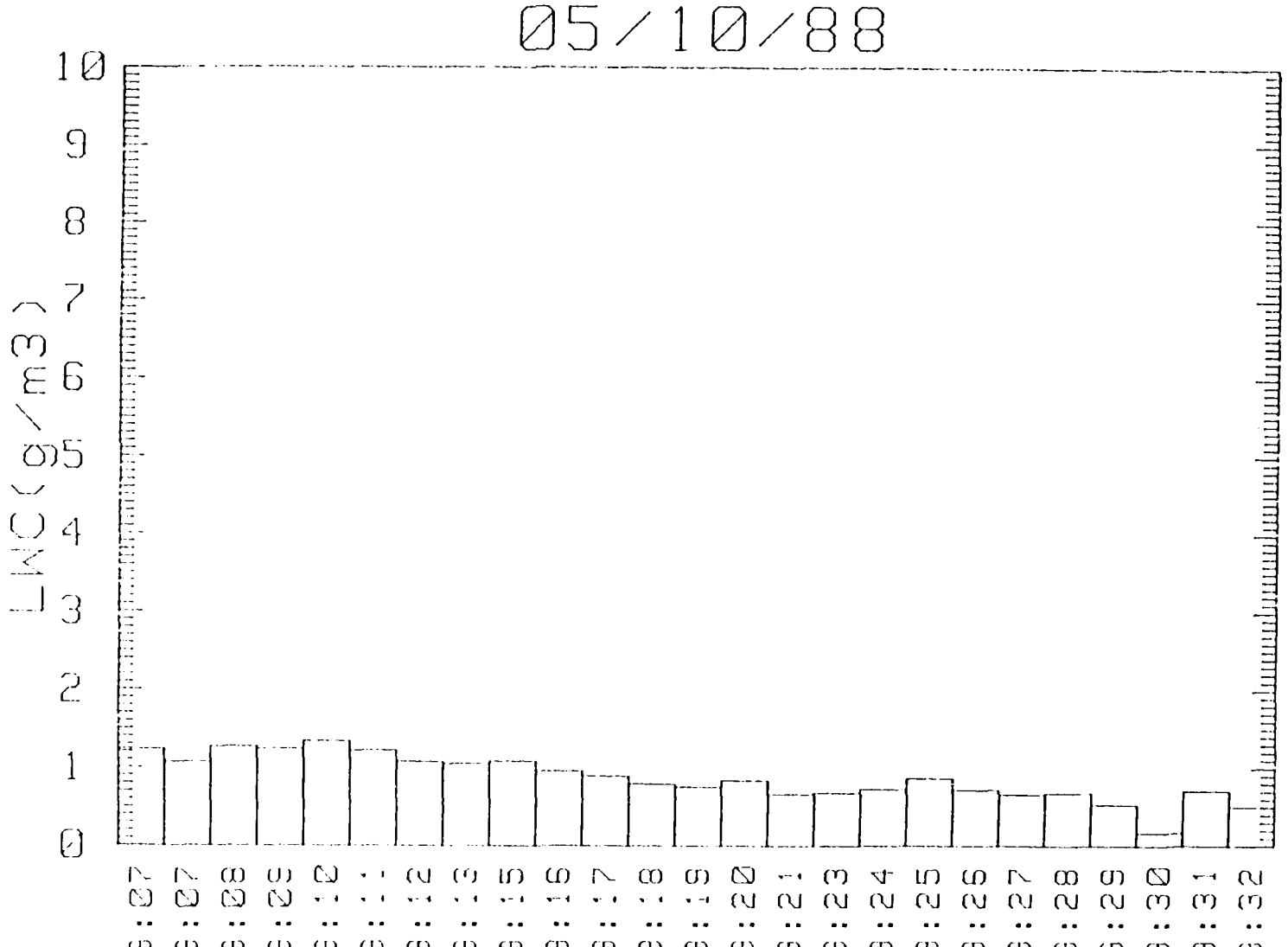
05/10/88
10
9
8
7
6
5
4
3
2
1
0
LMC(g/m3)
05:27
05:27
05:28
05:28
05:12
05:11
05:12
05:13
05:15
05:16
05:17
05:18
05:19
05:20
05:21
05:23
05:24
05:25
05:26
05:27
05:28
05:29
05:30
05:31
05:32